71-0225-00-01

STUDY OF AUTOMATIC AND MANUAL TERMINAL GUIDANCE AND CONTROL SYSTEMS FOR SPACE SHUTTLE VEHICLES

FINAL REPORT SUPPLEMENT
(APRIL 1971 THROUGH JUNE 1971)

DECEMBER 1971

BY

STEPHEN OSDER
ROGER KELLER

PREPARED FOR
NATIONAL AERONAUTICS AND SPACE ADMINISTRATION
AMES RESEARCH CENTER
MOFFETT FIELD, CALIFORNIA
PER CONTRACT NAS2-5804

PREPARED BY
SPERRY FLIGHT SYSTEMS DIVISION
SPERRY RAND CORPORATION
PHOENIX, ARIZONA

TABLE OF CONTENTS

LIST OF ILLUSTRATIONS

SECTION I

INTRODUCTION

This report supplement summarizes work accomplished on NASA Contract NAS2-5804, following completion of the original tasks for the study of Automatic and Manual Terminal Guidance and Control Systems for Space Shuttle Vehicles. The original tasks involved design studies and simulator evaluations using four different candidate vehicles as the test bed for demonstrating system concepts and performance. As NASA's Phase B Design Studies for the space shuttle progressed, these four vehicles rapidly became obsolete. During 1970 and 1971, the life expectancy of a space shuttle configuration was about 3 months. In order to keep the study being performed on Contract NAS2-5804 from becoming a series of simulator programming exercises as new space shuttle configurations evolved, the vehicle models for this study were frozen in September 1970. A Low Cross Range (LCR), straight-wing vehicle designed by McDonnell Douglas was used as the candidate of the straight-wing class, while a High Cross Range (HCR) delta configuration designed by North American Rockwell was the selected vehicle of that class. The space shuttle program abandoned the LCR class of vehicle in the winter of 1970-1971. The NAR HCR orbiter configuration (frozen for this study in September 1970) was redesigned several times by NAR before and after the completion of their Phase B Design Study. The purpose of the work reported on in this supplementary report was to take another look at the emerging space shuttle designs in order to verify the applicability of the concepts developed in the previous work.

The supplementary study had three main objectives.

- Verify terminal guidance and control system performance with a 1971 space shuttle orbiter configuration.

- Refine terminal glide and flareout precision and speed management using drag brake modulation (previous vehicle aero models did not include drag brake characteristics) plus additional guidance law techniques suggested in the previous study.

- Determine the sensitivity of landing performance to vehicle L/D; identify how the guidance and control system variables should be adapted to cope with different vehicle lift and drag characteristics.

To achieve these objectives, a late version (April 1971) delta orbiter designed by McDonnell Douglas was used as the model vehicle. Guidance and control system parameters were adjusted for good performance with this vehicle and parametric studies involving L/D variations, starting with this vehicle, were performed to determine the L/D sensitivity.

This report summarizes the new vehicle aero characteristics, the guidance and control system parameters selected for this vehicle, the selected flight path geometry, the landing performance obtained with winds and turbulence, and the influence of vehicle L/D on that performance.

SECTION II

DISCUSSION

A. VEHICLE AERO MODEL

The McDonnell Douglas Astronautics Company (MDAC) delta orbiter, designated MDAC-255BJ0050-B, was the baseline vehicle for this study. The salient characteristics are summarized in Table 2-1.

TABLE 2-1

MDAC DELTA ORBITER CHARACTERISTICS (CIRCA FEBRUARY 1971)	
Weight (landing) - pounds	253,448
Wing Span (b) - feet	97.5
MAC ($\bar{c}$) - feet	62.9
I_{xx} - (slug-feet^2 x 10^6)	2.2
I_{yy} - (slug-feet^2 x 10^6)	12.74
I_{zz} - (slug-feet^2 x 10^6)	13.35
I_{xz} - (slug-feet^2 x 10^6)	-0.087
Ref Area (S) - feet^2	5,330
Wing Loading (W/S) - pound/feet^2	47.5
Peak L/D at Landing Condition	6.7
α for $(L/D)_{PEAK}$ (degrees)	7.5
*Pitch Control Power - M_{δ_e} (1/sec^2)	-2.26
*Roll Control Power - L_{δ_A} (1/sec^2)	5.07
*Yaw Control Power - N_{δ_R} (1/sec^2)	-0.335

*For Landing Condition, Q = 150 pounds/foot^2

The main difference (from the standpoint of terminal guidance), between this vehicle and the NAR design used in the previous work, is in the L/D characteristics. The MDAC vehicle has a lower L/D for the final approach flight conditions, about the same L/D as the NAR vehicle in the transonic regions and a slightly lower L/D at supersonic speeds. The peak-trimmed L/D characteristics of the MDAC and NAR vehicles are compared in Table 2-2.

TABLE 2-2

COMPARISON OF L/D_T FOR NAR AND MDAC HCR VEHICLES

NORTH AMERICAN HCR			MDAC HCR		
MACH NO.	PEAK L/D_T	ANGLE OF ATTACK	MACH NO.	PEAK L/D_T	ANGLE OF ATTACK
0.3	9.4	10.5	0.26	6.7	7.5
0.9	5.5	10.5	0.8	6.5	7.0 deg
1.2	3.0	11.0	1.1	3.0	6.5
2.0	2.5	11.5	2.0	2.15	10 deg

The aero data obtained indicates the vehicle is well behaved in pitch with only a slight pitch up occurring at higher angles of attack ($>$ 15 degrees). Laterally, however, the vehicle stability becomes very unpredictable. The dihedral effect (Figure 2-1), indicated primarily by the derivative C_{ℓ_β}, becomes very destabilizing in the lower transonic regions for angles of attack greater than 12 degrees. On the other hand, the directional stability (C_{n_β}) (Figure 2-2) becomes very stabilizing at these same conditions. For the subsonic and supersonic flight conditions (C_{n_β}) is erratic and tends toward instability at almost all angles of attack. It is noted that this characteristic of negative C_{n_β} is now considered typical of most space shuttle vehicle configurations. As discussed in the main report, lateral/directional stabilization for the negative C_{n_β} conditions is provided by lateral acceleration (A_y) feedback through the rudders. This requires reasonable rudder effectiveness. The required effectiveness is available at the supersonic and subsonic speeds involved in the terminal phase of flight. (At hypersonic speeds, where rudder effectiveness may disappear, this problem of static directional instability must be solved with the reaction control system.) The source of aero data was MDAC. The data used in this study was eventually published by McDonnell Douglas as Reference 11. (The references of the main report are reproduced in this supplement.)

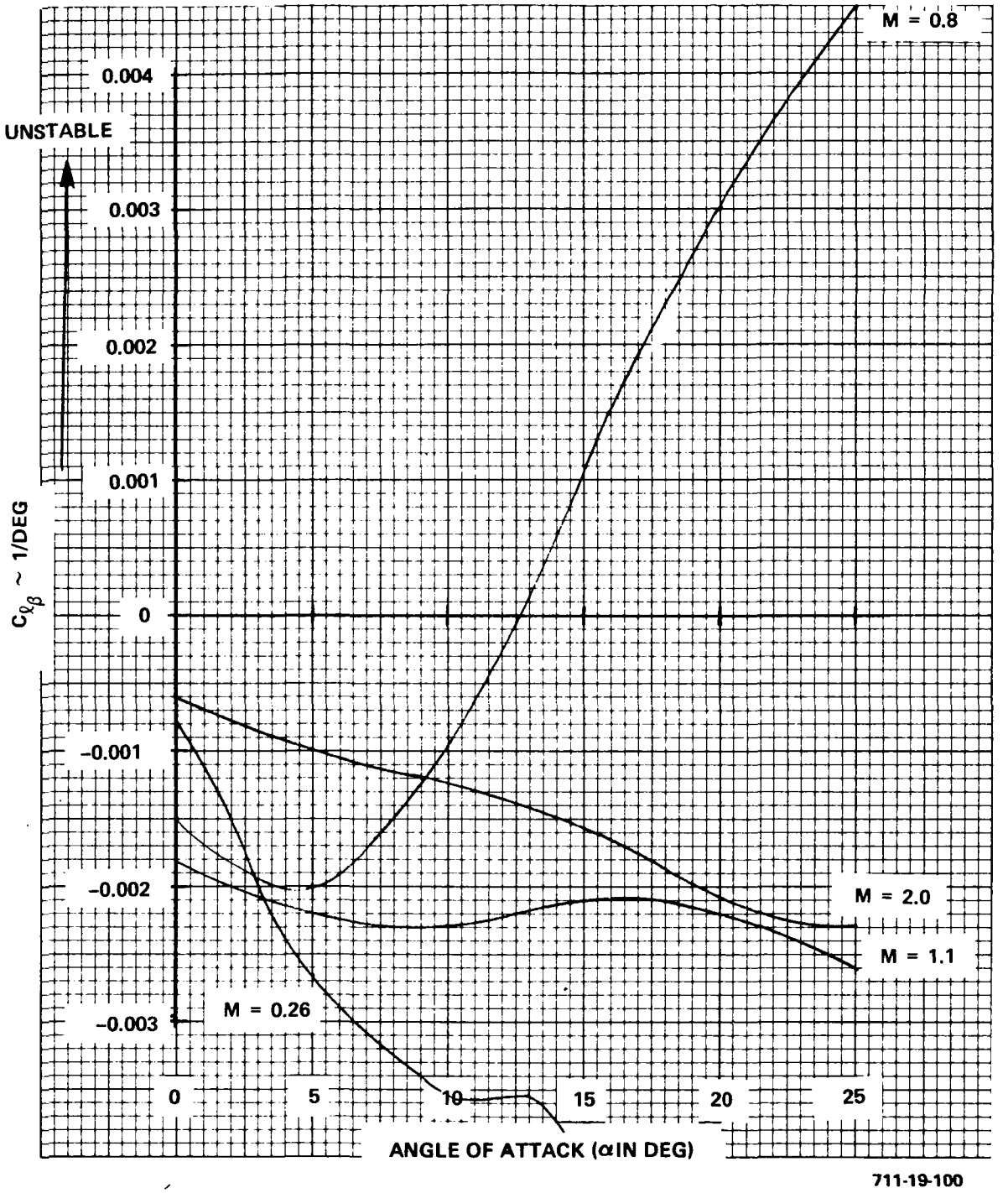

Figure 2-1
MDAC Delta Orbiter Lateral/Directional
Static Stability Derivatives
C_{ℓ_β} versus Angle of Attack for Different Mach Numbers

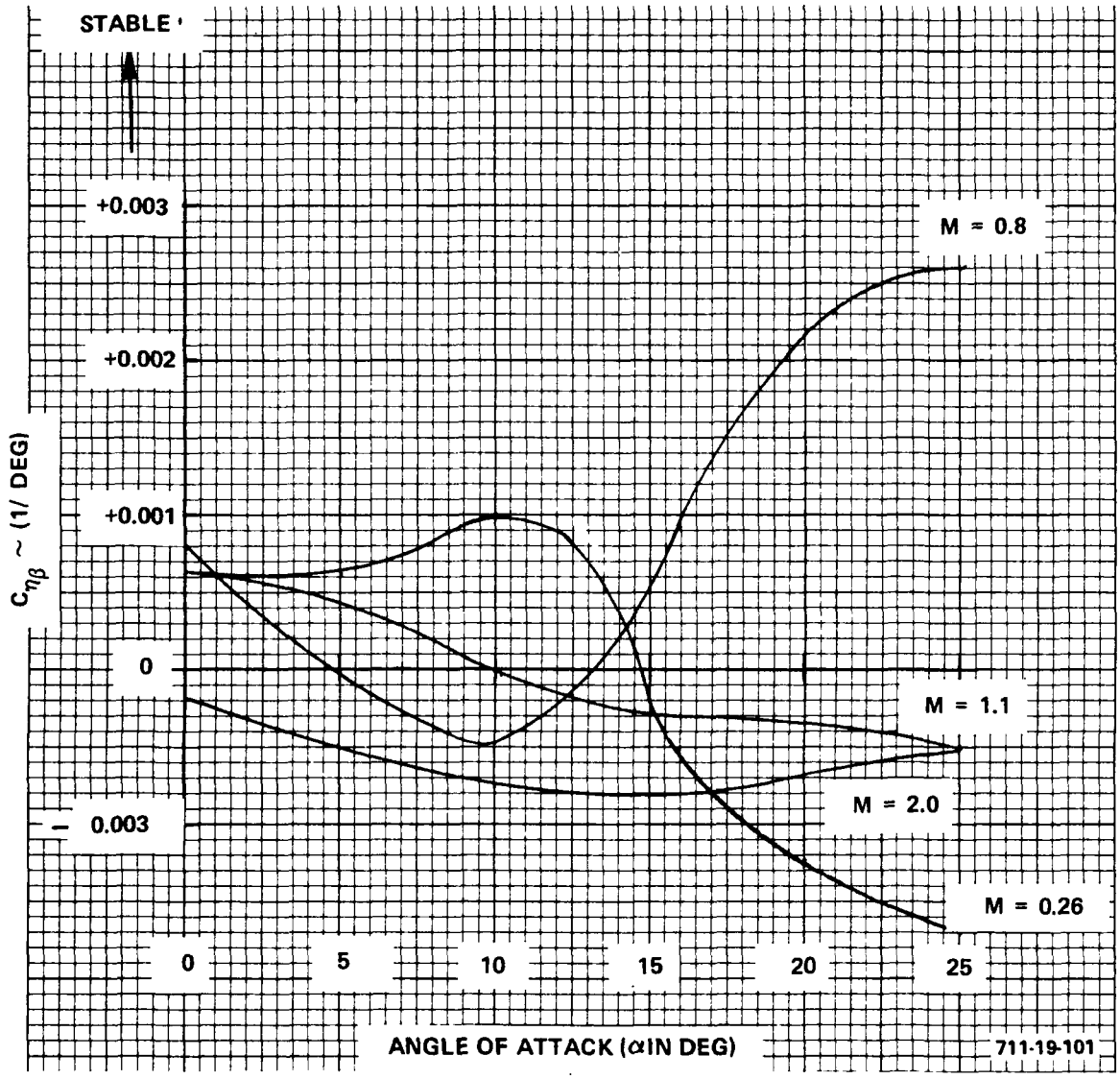

Figure 2-2
MDAC Delta Orbiter Lateral/Directional
Static Stability Derivatives
C_{n_β} versus Angle of Attack for Different Mach Numbers

B. GUIDANCE AND CONTROL SYSTEM PARAMETER SUMMARY

1. Autopilot Stabilization Loops

Attitude stabilization is achieved through symmetrical elevon control (pitch), differential elevon control (roll), and rudder (yaw). Figure 2-3 shows the elevon control system block diagram that identifies an equivalent aileron (δ_A) and elevator (δ_E) output with appropriate limits. The identification of an artificial elevator and aileron deflection is needed for compatibility with the definition of control surface moment and force coefficients. Note on Figure 2-3 that an aileron command summing into the asymmetrical elevon displacement limits can result in unbalanced pitch moments for some combinations of elevon trim and aileron command. The nominal trim elevon varies between -30 degrees and about -8 degrees so that this phenomenon does not occur during a trimmed pitch condition. There was no evidence of any problems of this type during simulations of combined pitch and roll maneuvers associated with the landing trajectories; but if they should ever prove to be a source of difficulty, the aileron displacement limit can be varied as a function of elevon trim to cause symmetrical limiting.

The elevator control law is identical to that used previously with other space shuttle configurations except for the gains.

$$\delta_{E_{COMMAND}} = k_\theta \left[(\theta - \theta_c) + \frac{k_q}{k_\theta} \left(\frac{\tau_1 s}{\tau_1 s + 1} \right) (q - q_c) \right] \left(1 + \frac{k_{INT}}{s} \right) + \delta_E (M, \alpha_{REF}) \quad (2\text{-}1)$$

where θ_c and q_c are pitch and pitch rate guidance or manual maneuver commands and $\delta_E (M, \alpha_{REF})$ represents a predictive trim command based on Mach and reference angle of attack.

The aileron and rudder control laws are also identical to those used previously.

$$-\delta_{A_{COMMAND}} = k_\theta (\theta - \theta_c) + \frac{k_p}{k_\theta} (p - p_c) \quad (2\text{-}2)$$

where θ_c and p_c are roll and roll rate guidance or manual maneuver commands.

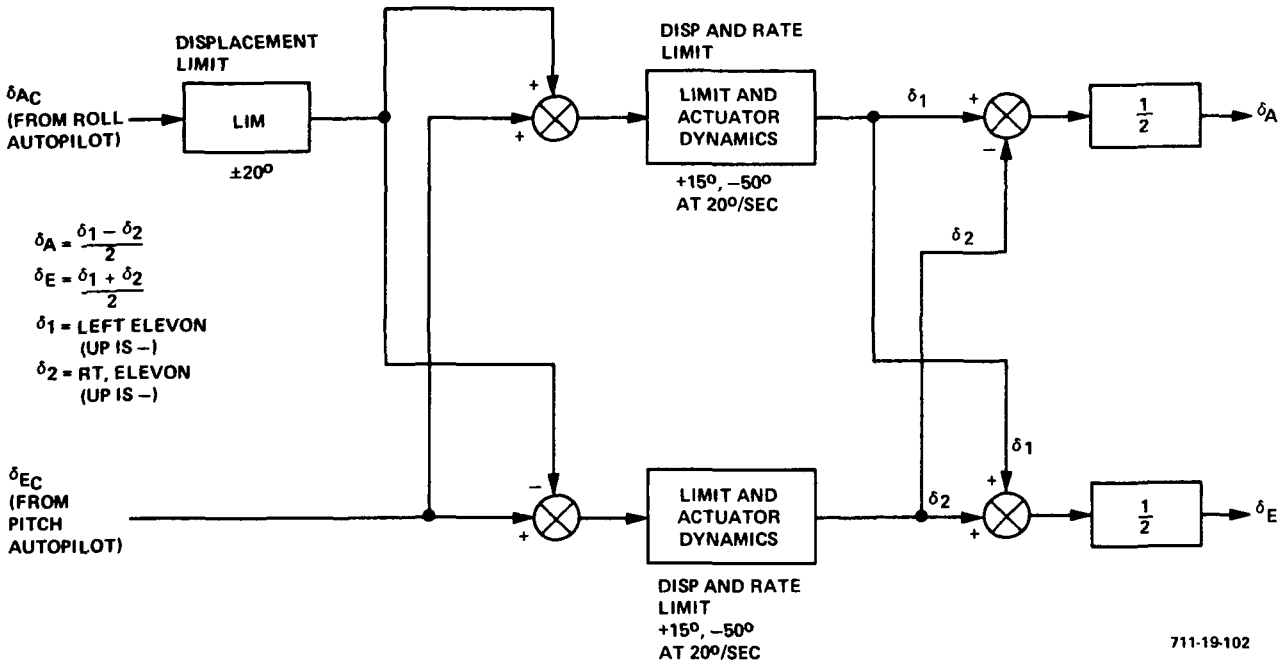

Figure 2-3
Elevon Control System

$$\delta_{R_{COMMAND}} = k_r \left[r - (g/V)\sin \phi_c\right] \frac{\tau_4 s}{\tau_4 s + 1} + \frac{k_{A_Y}}{\tau_5 s + 1} A_Y \qquad (2\text{-}3)$$

$$+ k_{RA}\, \delta_{AC} \frac{\tau_6 s}{(\tau_6 s + 1)(\tau_7 s + 1)}$$

The following gains and filter parameters were used for the MDAC vehicle:

$*k_\theta = 2.5$

$k_q/k_\theta = 1.0$

$\tau_1 = 2.5$

$k_{INT} = 0.1$

$k_p/k_\theta = 2.0$

$k_\theta = 1.50\ (\frac{130}{Q})$

$k_r = 12.0\ (\frac{130}{Q})$

$K_{AY} = (3)\ (\text{Mach})(\frac{130}{Q})$

$\tau_4 = 2.5$

$\tau_5 = 0.1;\ \tau_6, \tau_7, k_{RA} = 0$

*NOTE: A Q gain control is usually used; but for the MDAC flight conditions, a constant gain of 2.5 was found to be adequate.

δ_E (m, a_{REF}) was not used because it is intended primarily for hypersonic to subsonic transition programs. This phase of flight control was not optimized with the MDAC vehicle since this supplementary study concentrated on final approach and flareout.

2. Vertical Guidance Laws (not including flareout)

(Flareout and speed management guidance are discussed in a subsequent section.) Terminal glide path acquisition and tracking is initiated when the vehicle satisfies various criteria regarding approach to the glide path. For the MDAC vehicle, the glide path control equations were:

$$\theta_c = k_\gamma (\gamma_{REF} - \gamma) + k_h \left(h_{REF_1} - h\right)\left(1 + \frac{a_2}{s}\right) \tag{2-4}$$

where γ_{REF} is the glide angle of the reference glide path and h_{REF_1} is the instantaneous altitude reference corresponding to the center of the glide path. Constraints on θ_c are imposed to prevent excessive normal accelerations, angles of attack, and speed variations.

Various geometrical relationships between the steep and shallow glide path are possible for a given vehicle. The possibilities are increased when speed brake control adds an additional variable to the problem. (This subject is considered in greater detail later.) However, for the purpose of summarizing the vertical guidance laws, the steep glide slope is -12 degrees, the shallow glide path is -2.5 degrees, and the first flare is initiated at a nominal altitude of 1500 feet (where the nominal velocity is 595 ft/sec). First flare is initiated at altitude h_2 where h_2 is determined by the following equation:

$$h_2 = h_{NOM}\left(1 + C_1 \frac{\Delta V}{V_{NOM}}\right) \tag{2-5}$$

where

h_{NOM} = 1500 ft

V_{NOM} = 595 ft/sec

C_1 = 0.16

At first flare, the following pitch command is inserted:

$$\theta_c = k_\gamma (\gamma_{REF} - \gamma) + \int_{t=t_o}^{t_x} \dot{\theta}_c\,(t)\,dt + \theta_{p_1}\,(t) \tag{2-6}$$

where

$$\gamma_{REF} = \gamma_1 + \int_0^{t_x} \dot{\gamma}_c\,(t)\,dt \tag{2-7}$$

$$\dot{\gamma}_c\ (t) = \dot{\theta}_c\ (t) = 57.3\ \frac{N_{ZMAX}}{V}\ \text{deg/sec} \tag{2-8}$$

$$N_{ZMAX} = +16\ \text{ft/sec}^2$$

$$t_x = \text{time at which} \quad \dot{\gamma}_c\ dt = \Delta\gamma_{REF} = -2.5\ \text{deg} - (-12\ \text{deg}) = 9.5\ \text{deg} \tag{2-9}$$

where

$-2.5\ \text{deg} = \gamma_{REF_1}$ (shallow glide slope)

$-12.0\ \text{deg} = \gamma_{REF_2}$ (steep glide slope)

$\theta_{p_1}\ (t)$ is a predictive term equal to

$$\theta_{p_1}\ (t) = \int_o^t \dot{\gamma}_c\ dt + 57.3\ \frac{d_1}{Q}\left(1 - \frac{\Delta\gamma\ \sin\gamma}{N_{ZMAX}}\right) - 57.3\ d_2 \int_o^t \left(\frac{\dot{V}}{V}\right)\frac{1}{Q}\ dt \tag{2-10}$$

which may be simplified to

$$\theta_{p_1}\ (t) = \int_o^t \dot{\gamma}_c\ dt + \frac{57.3}{Q}\left[d_1 - d_2 \int_o^t \left(\frac{\dot{V}}{V}\right) dt\right] \tag{2-11}$$

where d_1 and d_2 are constants

Closed-loop tracking of the shallow glide path (defined by h_{REF_2}) is initiated when:

- Altitude is below the shallow glide slope and the descent is steeper than γ_{REF_2}

$$h_{E_2} \geqslant 0 \text{ and } \gamma \leqslant \gamma_{REF_2} \tag{2-12}$$

$$\left(h_{E_2} = h_{REF_2} - h\right)$$

or

- Altitude is above the shallow glide slope and the descent is shallower than γ_{REF_2}

$$h_{E_2} \leq 0 \text{ and } \gamma \geq \gamma_{REF_2} \tag{2-13}$$

The closed loop tracking equation for the shallow glide path is identical to that used for the steep glide path, except for predictive commands that compensate for the deceleration and gear deployment. The tracking equation is:

$$\theta_c = k_\gamma \left(\gamma_{REF_2} - \gamma\right) + k_h h_E \left(1 + \frac{a_2}{s}\right) + \theta_{p_2} \tag{2-14}$$

where, as in the case of the steep glide path tracking, k_h varies inversely with velocity.

$$\theta_{p_2} = -57.3 \frac{d_1}{Q}\left(1 - \frac{\Delta_\gamma \sin\gamma}{N_{ZREF}}\right) - 57.3\, d_3 \int_o^{t_{FF}} \left(\frac{1}{Q}\right)\left(\frac{\dot{V}}{V}\right) dt \tag{2-15}$$

The first part of θ_{p_2} cancels the identical term that existed during the flare maneuver. The cancellation is necessary if the guidance computer uses the previous value of θ_c as the initial condition for mode transition.

The gains used for the MDAC vehicle were:

k_γ (for steep and shallow glide paths) = 1.0 deg/deg

k_h (for steep glide path control) = 0.06 deg/ft

k_h (for shallow glide path control) = $0.067 \left(\frac{500}{v}\right)$ deg/ft

$d_1 = 12.8$

$d_2 = 77.0$

$d_3 = 88.0$

3. Lateral Guidance

The control law to the lateral flight path reference (localizer) is

$$(\Delta y + k_{\dot{y}} \dot{y})\ k_y = \phi_c \tag{2-16}$$

This control is initiated after a proper intercept path has been established and Δy and $\dot{y}$ are below specified thresholds. Note that Δy and $\dot{y}$ are smoothed quantities. That is, if y and $\dot{y}$ are obtained from radio navigation computations, the quantities used in the control law should be smoothed using low-pass filtering of the radio-derived information with signal bandwidth restored with short-term inertial data. The radio information provides the low frequency content of the control signals, while the inertial information provides the higher frequency content of Δy and $\dot{y}$.

Thus far in these studies, an integral control term in the lateral control equation has not been used (integral of Δy). It is common practice in aircraft lateral guidance systems to use integral control of the Δy error to correct for estimation errors in $\dot{y}$. Integral control on Δy also helps minimize lateral errors resulting from crosswind shears. However, if integral control is used, it is essential that it be activated only when Δy errors are very near zero because a long period oscillatory mode is created by the addition of the integral loop. That mode is tolerable if the maximum amplitude of the errors can be held to very small values, as they are after a tight lateral tracking phase has been established.

The gains used with the MDAC vehicle were:

$$k_{\dot{y}} = 20$$

$$k_h = 0.03 \text{ deg } \phi_c/\text{ft}$$

Note that these gains were the same as those used for all previous vehicles studied. Stability analyses indicate that k_y can be increased to about 0.06 to 0.1 in order to improve control tightness. Since detailed investigations of lateral dispersions were not made, this higher gain was not evaluated. However, with the assumption that inertially smoothed $\dot{y}$ and Δy data is available, the higher gains should be used in any further studies of lateral guidance performance.

C. FLIGHT PATH GEOMETRY AND SPEED MANAGEMENT

1. High Altitude Guidance

The high altitude lateral steering (energy management) equations developed for the NAR delta orbiter were used with the MDAC vehicle. The system allowed the MDAC vehicle to acquire the terminal glide path by the time an altitude of 20,000 feet was reached. However, no attempt was made to determine the size of the energy management window or to optimize the stored nominal trajectory [Equation (3-98) of the main report for this study]. For pitch guidance, a Q loop was used with the Q reference established by an angle-of-attack program [as described in the main report, Equations (3-92) through (3-96)]. This type of pitch guidance had not been used previously in the studies with the NAR vehicle. The guidance equations were:

$$\theta_c = K_Q \left(Q - Q_{REF}\right) \left(1 + \frac{a}{s}\right) + K_L \left(\frac{1 - \cos \phi_c}{\cos \phi_c}\right) \tag{2-17}$$

where

$$Q_{REF} = Q_{NOM} + \Delta Q \tag{2-18}$$

$$\Delta Q = \frac{k_\alpha}{s} (\alpha - \alpha_{REF}) \tag{2-19}$$

$$\alpha_{REF} = f\ (M, h, \Delta E)$$

For the MDAC vehicle, α_{REF} was made only a function of Mach (M). The function of altitude (h) and energy error (ΔE) is retained in the guidance equation, but zero values were used thus far. The α reference was made the function of Mach, which resulted in peak L/D. A typical descent from 100,000 feet using this type of pitch guidance is illustrated in Figure 2-4. Note that the dynamic pressure converges toward about 150 pounds per feet^2 in the supersonic Mach 2.0 to 1.0 region, but then changes in the transonic region. The flight path angle (γ) reaches about -11.0 degrees, and then, as the lift coefficient increases in the transonic region, it shallows back toward about -7.0 degrees. The guidance law contained logic that would have locked on to γ control if the reference terminal glide γ of -12 degrees had been reached. In previous work with the NAR vehicle, where a terminal glide angle of -10 degrees was used, the pitch guidance system always ended on γ control prior to intercepting the terminal glide path.

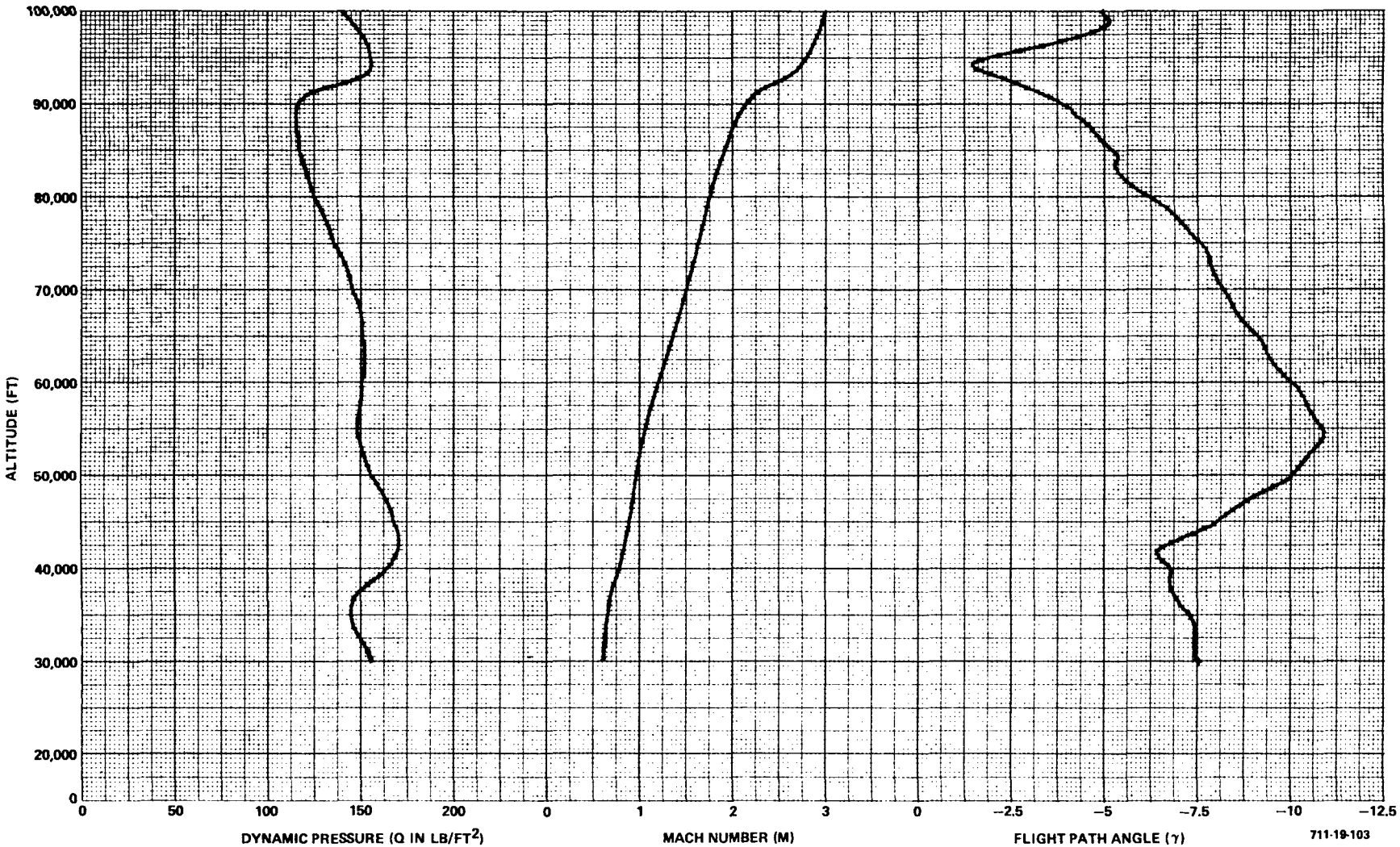

Figure 2-4
MDAC Delta Vehicle High Altitude Descent
(Typical Straight - In Approach)

2. Terminal Glide Path Geometry and Speed Brake Control

Figure 2-5 shows the equilibrium flight path angle versus airspeed for the MDAC and NAR delta orbiters. A steeper equilibrium flight path angle is required to fly the MDAC HCR orbiter and remain well on the front side of the L/D curve. This results from the lower L/D for the MDAC vehicle. It is noted that the reference to the NAR vehicle relates to the vehicle used in the previous simulations.

Simulator runs were taken to determine the MDAC vehicle's terminal glide and flareout characteristics without speed brakes. These runs were aimed at defining the speed convergence characteristics of this vehicle after it acquires the steep glide path. Figure 2-6 is a velocity/altitude plot from 20,000 feet to touchdown. Three significantly different initial velocity conditions (M = 0.5, 0.7, 0.9) at 20,000 feet were investigated to determine the velocity convergence on a glide path of -11 degrees. At flare onto the 2.5-degree flight path (altitude $\approx$ 1750 feet), the velocities have converged to within ±15 feet per second, with the nominal landing at -1.8 feet per second. The touchdown velocities varied from 177 to 184 knots.

Figure 2-6 indicates that the speed convergence of the MDAC delta wing vehicle toward an equilibrium speed on the steep glide path is relatively good. However, in headwind and tailwind conditions, constraining the vehicle to the fixed glide path results in a significant velocity spread at touchdown. Speed brakes are needed to minimize the effect of winds on touchdown velocity.

Two possible speed brake control techniques were investigated.

- Below 20,000 feet, deploy speed brakes to a nominal position (about 25 to 50 percent). Modulate speedbrakes about this equilibrium position in order to maintain a desired reference airspeed.

- Select a desired equilibrium speed that can be flown with zero speed brake deployment in a nominal headwind condition. Deploy speed brakes only for excess speed conditions.

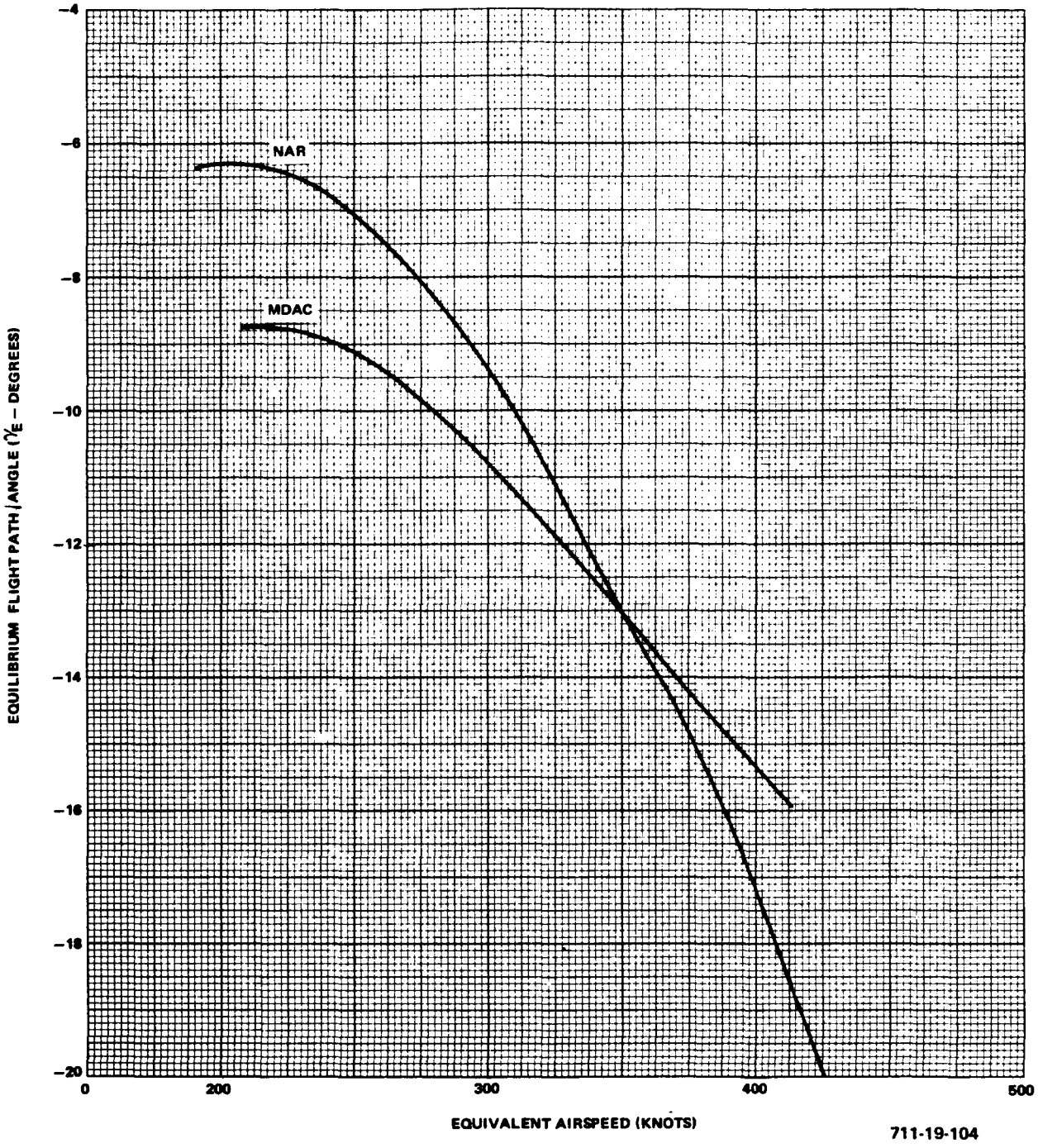

Figure 2-5
Equilibrium Flight Path versus Equivalent Airspeed
MDAC and NAR Delta Orbiters

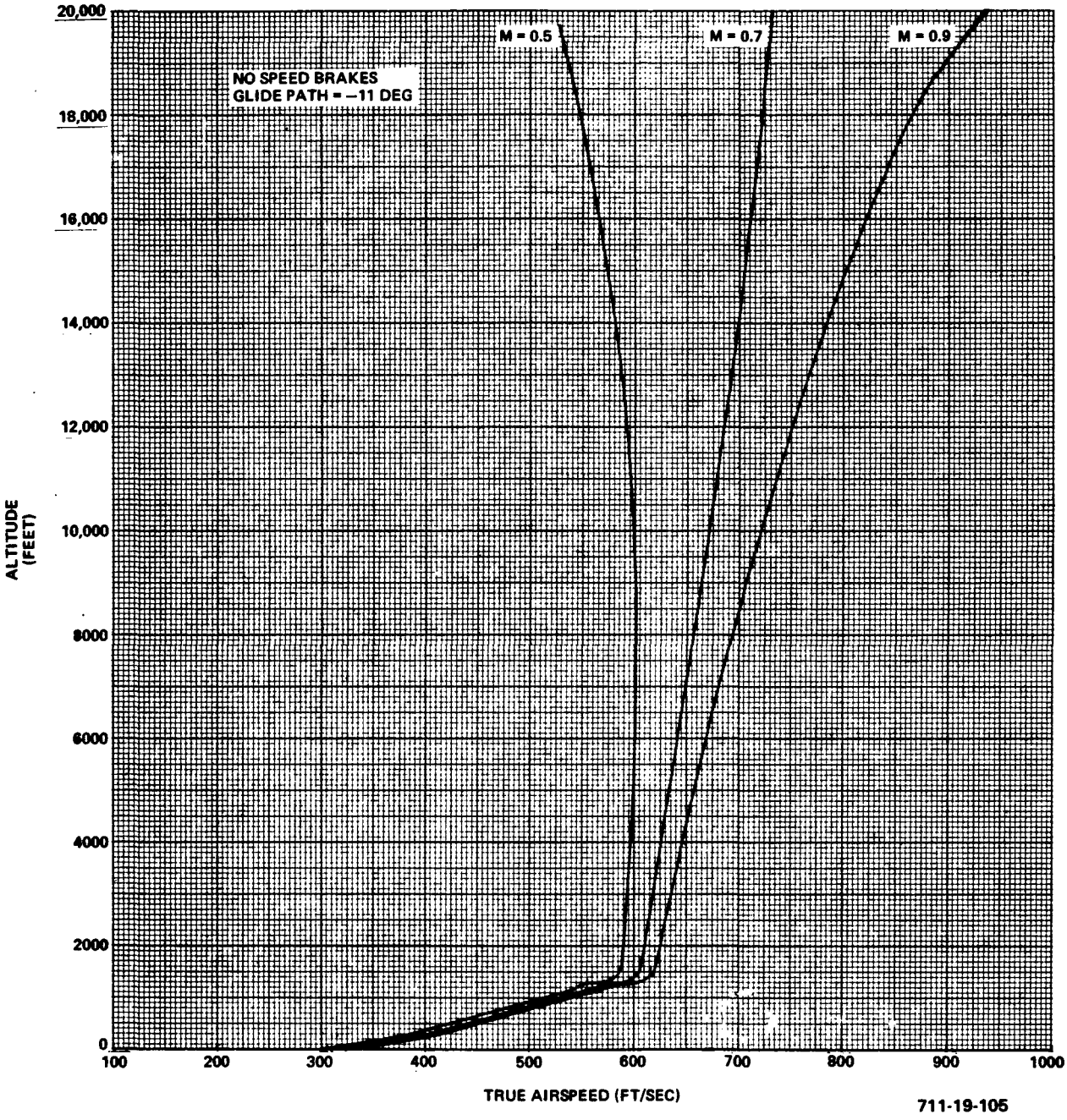

Figure 2-6
MDAC HCR Orbiter Velocity, Altitude Histories

The trade-off between these methods is reduced shallow glide (float) capability (first method) versus excessive approach speed for the second method. In previous studies with the NAR HCR vehicle, the low drag, high L/D characteristic of that vehicle permitted an extended shallow glide control phase starting at about 1200 feet. Attempting to achieve the same length of shallow glide path control with the MDAC delta-wing vehicle requires a high velocity at first flare (as it did for the NAR vehicle). In order to obtain this speed, the approach flight path for the higher drag MDAC vehicle was steepened to -12 degrees from the -10-degree value used in the previous delta-wing vehicle study.

Figure 2-7 shows the flight path geometries associated with above-referenced drag brake methods. For the second method to yield a 1200-foot run on the shallow glide path, the equilibrium speed at first flare was about 350 knots (probably excessive). If the second method was mechanized with 25-percent nominal speed brake deployment, the resulting speed was too low to maintain a significant shallow glide path tracking phase. A drag brake control loop using 300 knots as the reference airspeed can acquire the shallow glide path at about 700 feet. If the speed reference is lowered to 250 knots, the capability for a shallow glide path tracking phase is eliminated.

Figure 2-8 is an altitude/airspeed recording of approach and landing runs using speed brake control for three diverse initial speed conditions at 20,000 feet where the -12-degree glide path is acquired. The particular case illustrated in this figure represents the high speed upper bound for an approach. The airspeed reference maintained by the speed brake control loop is 350 knots. (The trajectory for the more reasonable speed case of 300 knots is indicated with an arrow on this figure.) The three initial conditions at 20,000 feet are:

M = 0.9 With tailwind at low altitudes and high altitude winds (90 degrees - West to East), which results in a 45-degree headwind

M = 0.7 With no winds

M = 0.5 With headwind at low altitudes and high altitude winds (90 degrees - West to East), which results in a 45-degree headwind

(Winds used were mean winds as defined in the Appendix. Note that low altitude headwind and tailwinds shear to zero at zero altitude. At 10 feet of altitude the headwind is 12.5 knots and tailwind is 5 knots. At 400 feet, the headwind is about 23 knots and tailwind is about 9 knots.)

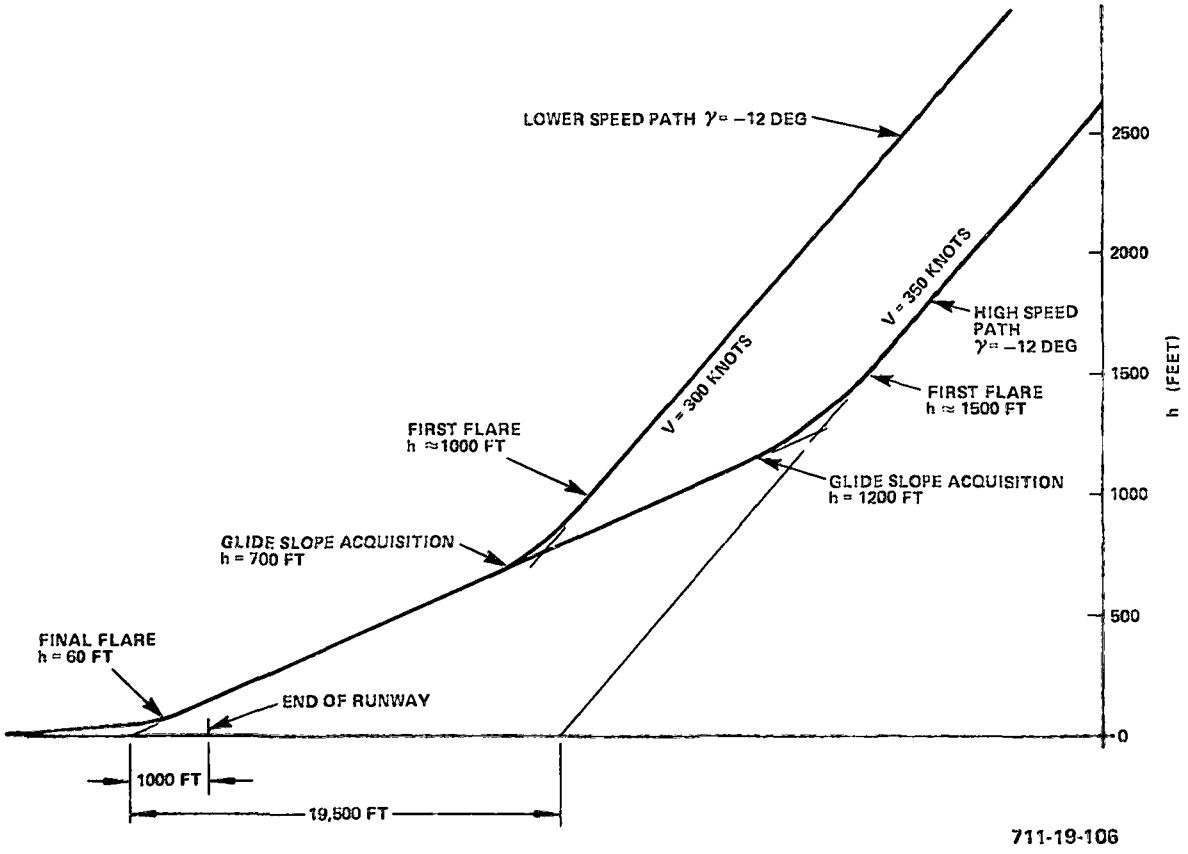

Figure 2-7
Two Possible 12-degree Final Approach Trajectories
(MDAC Delta Wing Vehicle)

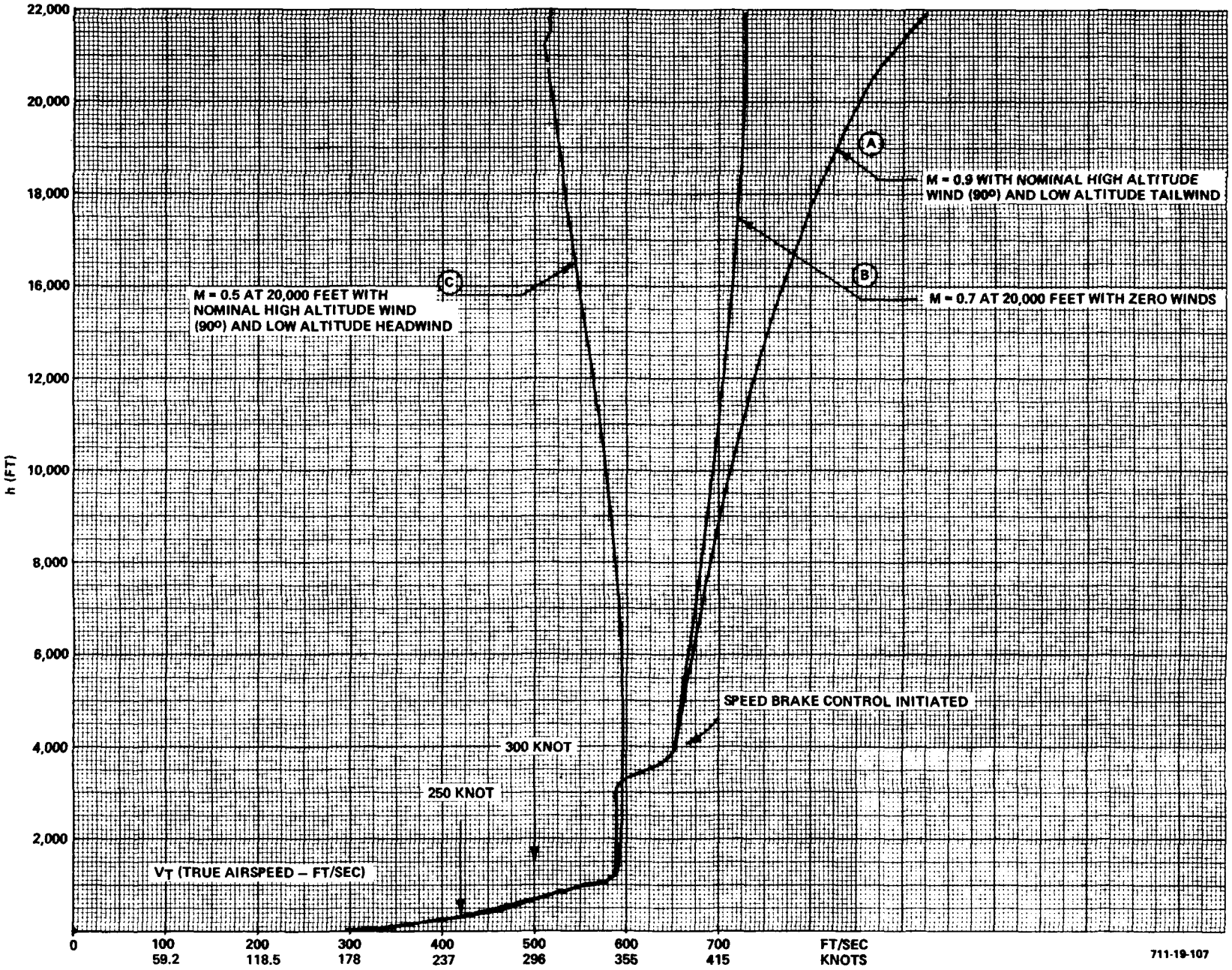

Figure 2-8
Altitude/Velocity Histories of Approach and
Landing Runs with Speed Brake Control

To demonstrate the effectiveness of the speed brake controls, they are not deployed until an altitude of 4,000 feet is reached. The speed variation prior to speed brake deployment is the result of two factors:

- The normal tendency to converge to a constant calibrated airspeed as the flight path angle is constrained
- The wind shear effects of the high-altitude and low-altitude winds

Note that the large speed decrease for the M = 0.9 case at altitudes between 10,000 and 20,000 feet is the result of the high-altitude (jet stream) wind, which is predominantly a headwind for the 224-degree approach path.

When speed brake control is initiated at 4,000 feet, a speed error of about 50 feet per second is brought to zero in about 400 feet of altitude. The simple proportional control law used was:

$$\delta_{SB} = (V - V_{NOM_1}) K_{SB_1} \tag{2-21}$$

$$\text{for } h_{1st\ FLARE} < h_{cg} < 4{,}000 \text{ ft} \tag{2-22}$$

where

V_{NOM_1} = 595 ft/sec

K_{SB_1} = 1.0 deg/ft/sec

$h_{1st\ FLARE} \approx$ 1500 ft = altitude of first flare

V = true airspeed

(Note that if speed brakes were deployed at higher altitudes, the parameter to be controlled should be calibrated airspeed, V_c, rather than true airspeed.)

For improved performance at a lower speed reference where a steady-state deployment is needed (rather than zero steady-state δ_{SB} for the 350 knot case), an integral loop would be useful. Thus K_{SB_1} would be replaced by K_{SB_1} $(1 + 0.1/s)$.

On the shallow glide slope, the speed brakes are deployed in accordance with a programmed velocity reference. The control law is:

$$\delta_{SB} = (V - V_{NOM_2}) K_{SB_2} \tag{2-23}$$

$$\text{for } 100 \text{ ft} < h_{cg} < 500 \text{ ft} \tag{2-24}$$

where

$$V_{NOM_2} = K_1 h_{cg} + K_2 \tag{2-25}$$

K_{SB_2} = 2.0 deg/ft/sec

K_1 = 0.32 (1/sec)

K_2 = 318 ft/sec

Note that the speed brakes were retracted during the first flare maneuver and during the initial phases of the shallow glide slope acquisition and tracking. They were also retracted at an altitude of 100 feet (at the maximum rate) to eliminate brake deflection at final flare. It was found advantageous to avoid any speed brake activity during final flare because of the extreme sensitivity of the flareout to speed brake variations. The linear velocity change program used on the shallow glide path is a simple approximation that gave good results. The refinement of speed brake deployment techniques through the use of a stored velocity versus altitude programs or other techniques that can converge all landings to within very narrow velocity dispersions must await additional refinement of the vehicle design and detailed study of operational procedures. Using the simple system described in this report, the velocity dispersion at touchdown was within 15 feet per second (9 knots) ranging from 295 to 310 feet per second (175 to 184 knots). Note that much of this dispersion occurred after the speed brakes were retracted at 100 feet. For the three diverse cases illustrated in Figure 2-8, the touchdown rate of descent ranged from -1.6 to -2.1 feet per second with runway dispersion within 100 feet. For all runs, the maximum speed brake deployment required was 30 degrees, which corresponds to about 50-percent authority.

3. Flareout Guidance

An extensive investigation of the final flare control laws was performed in an attempt to improve the touchdown dispersion experienced in the previous studies with the NAR vehicle. Previous results with the NAR vehicle indicate that, although the closed-loop controller:

$$\theta_{c_1} = K_{\dot{h}} \left(\dot{h}_{REF} - \dot{h} \right) \left(1 + \frac{a}{s} \right) - K_{\ddot{h}} \ddot{h} \tag{2-26}$$

with constant predictive commands

$$\theta_{c_2} = \frac{f_1}{1 + \tau s} + \int \frac{57.3}{V} f_2 dt \tag{2-27}$$

yielded good touchdown rates of descent under wind conditions, the longitudinal dispersion needed improvement.

Four areas of improvement were considered.

- Optimize vertical speed dynamic response; eliminate tendency to overshoot the touchdown vertical speed reference.
- Optimize the flare initiate correction law; select the proper sensitivity of Δh for flare-initiate-per-feet-per-second deviation from nominal $\dot{h}$.
- Correct the predictive flare maneuver command as a function of off-nominal vertical speed and forward speed.
- Adjust touchdown vertical speed reference as a function of deviation from a nominal $\dot{h}$ versus h maneuver; this trades off a harder landing against excessive runway dispersion.

The first three items provided the desired level of performance for the MDAC vehicle. The first involved tightening the closed loop $\dot{h}$ control system and matching the predictive pitch maneuver so that the reference $\dot{h}$ (-2 feet per second) is achieved at the desired altitude. Overshooting the -2-feet-per-second reference or achieving it at too high an altitude results in excessive runway consumption.

The second item (flare initiate correction) requires a proper gain that relates $\dot{h}$ variation to a change in the flare initiate point. In previous work with the NAR vehicle, $\dot{h}$ correction sensitivity was too high and the resultant effect was an overcompensation of flare initiation altitude for off-nominal vertical speeds. The proper equation for the MDAC vehicle and the specific flareout control laws used is

$$h_F = \text{altitude at which flare is initiated} \tag{2-28}$$

$$= h + \dot{h} - 45 \leqslant 0$$

The third correction item involves adjusting the predictive part of the flareout maneuver rather than use a constant term as in previous work. The predictive term includes a filtered step plus a ramp. The ramp already included a velocity compensation term. The total predictive command is

$$\theta_{CP} = \theta_{CP_1} + \theta_{CP_2} = \frac{f_1}{1 + \tau s} + f_2 \int \left(\frac{57.3}{V}\right) dt \tag{2-29}$$

The adjustment was made on f_1 as follows.

$$f_1 = f_1' + \left(\dot{h}_{REF} - \dot{h}_o\right) K_5 + \left(V_{REF_o} - V_o\right) K_6 \tag{2-30}$$

where

f_1' = Nominal maneuver magnitude (equal to 1.5 degrees for the MDAC vehicle

$\dot{h}_{REF_o}$ = Nominal vertical speed at flare initiate ($t = t_o$) = -15 ft/sec

$\dot{h}_o$ = Actual vertical speed at time of flare initiate

V_{REF_o} = Nominal airspeed at flare initiate = 345 ft/sec

V_o = Actual airspeed at flare initiate

For the MDAC vehicle, the optimum gains were

$$K_5 = -0.3 \text{ deg/ft/sec}$$

$$K_6 = +0.09 \text{ deg/ft/sec}$$

The complete pitch command equation for flareout is

$$\theta_c = -K_{\ddot{h}} \ddot{h} + k_{\dot{h}} \left(\dot{h}_{REF} - \dot{h} \right) \left(1 + \frac{K_I}{s} \right) + \theta_{cp} \qquad (2\text{-}31)$$

where

$K_{\ddot{h}} = 0.2 \text{ deg/ft/sec}^2$

$K_{\dot{h}} = 0.35 \text{ deg/ft/sec}$

$K_I = 0.5 \text{ deg/sec/deg}$

$\dot{h}_{REF} = -2 \text{ ft/sec}$

The h versus $\dot{h}$ phase planes for three landings corresponding to the three trajectories illustrated in Figure 2-8, are given in Figure 2-9. Touchdown occurs when cg height is 22 feet. These three landings involved a touchdown rate of descent variation of -1.6 to -2.1 feet per second (or a total spread of 0.5 foot per second about the nominal). All three landings touched down with a total runway dispersion of about 100 feet.

Using these control laws, 30 runs were made under headwind and tailwind conditions including wind shears and turbulence. (Winds and turbulence models used are defined in the Appendix.) The major contributor to variation in nominal touchdown $\dot{h}$ and runway position was the turbulence. Figure 2-10 plots these two critical touchdown parameters to demonstrate a performance plane for these 30 landings. The spread about the nominal is reasonable for both x and $\dot{h}$ with only one large x value (2000 feet from glide slope intercept) as possibly excessive. Figure 2-11 summarizes these landings with an $\dot{h}$ and x histogram. (The touchdown distance given here is measured from the glide slope intercept.) The average touchdown distance given here is measured from the glide slope intercept.) The average touchdown $\dot{h}$ was -2.83 feet per second, and the average x from glide slope intercept was 643 feet. In general, this represents good performance, but the sample size does not permit any statistically significant conclusions to be drawn at this time.

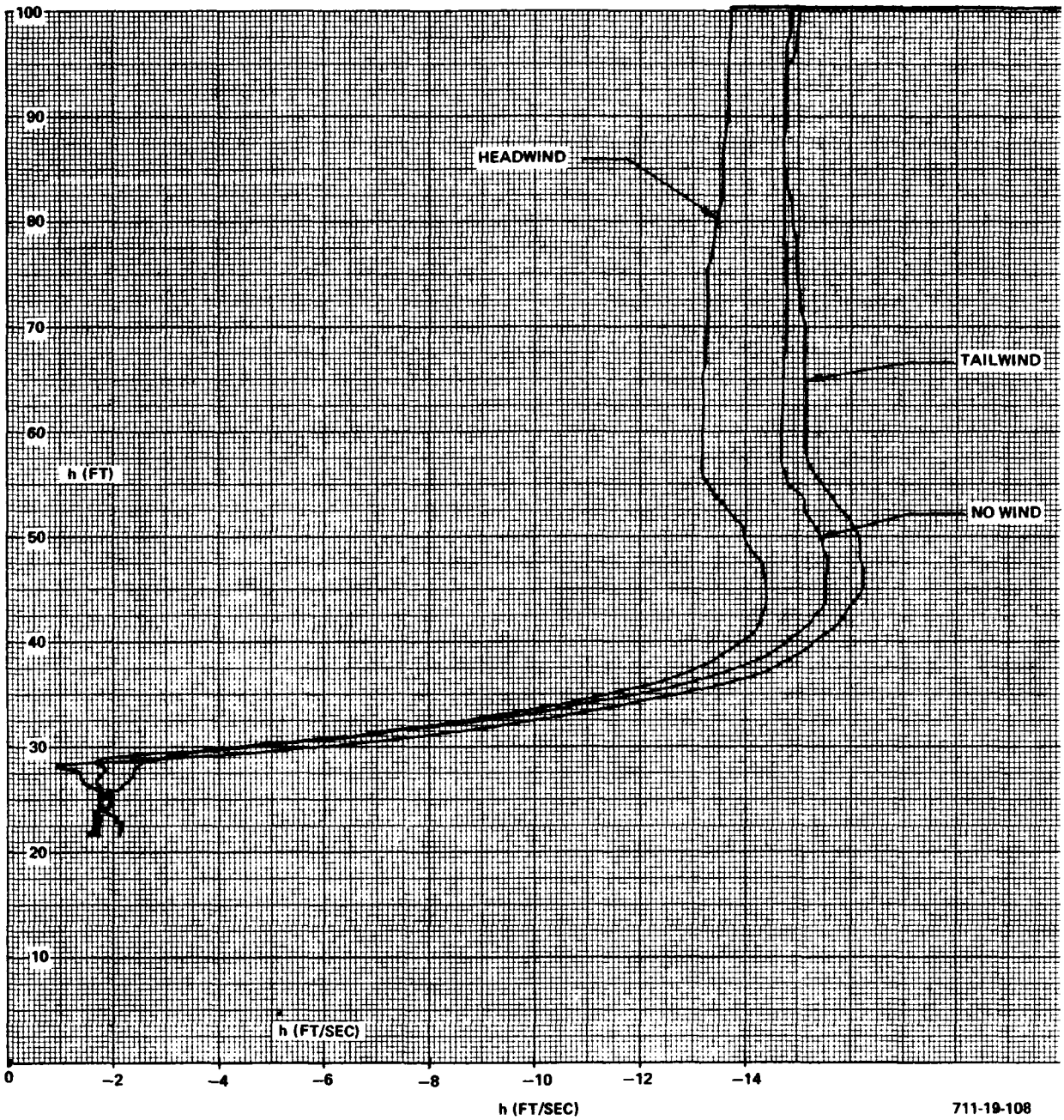

Figure 2-9
Flareout Trajectories for Three Diverse Initial
Speed and Wind Conditions

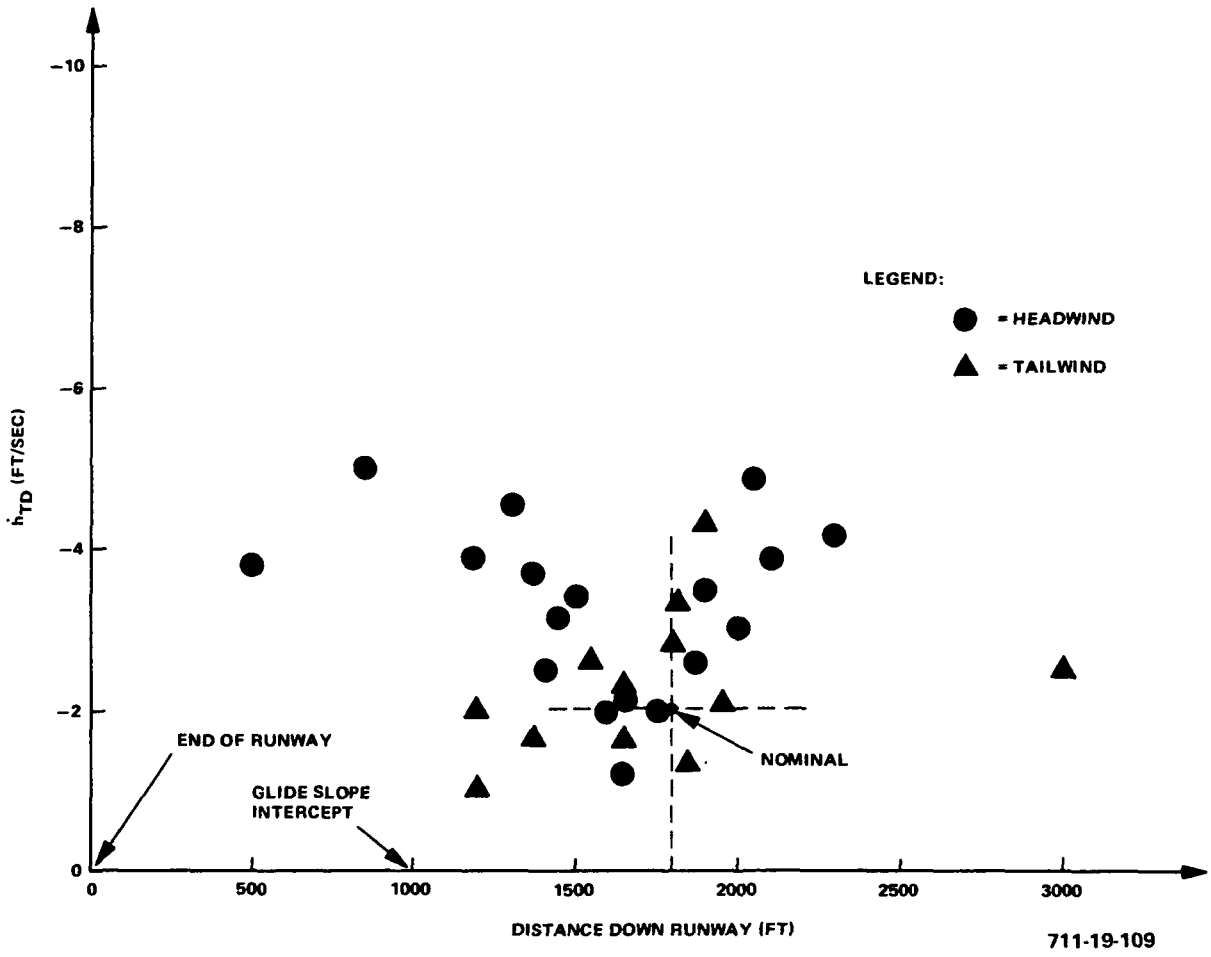

Figure 2-10
Landing Vertical Speed/Position Performance Plane,
30 Landings with Winds and Turbulence

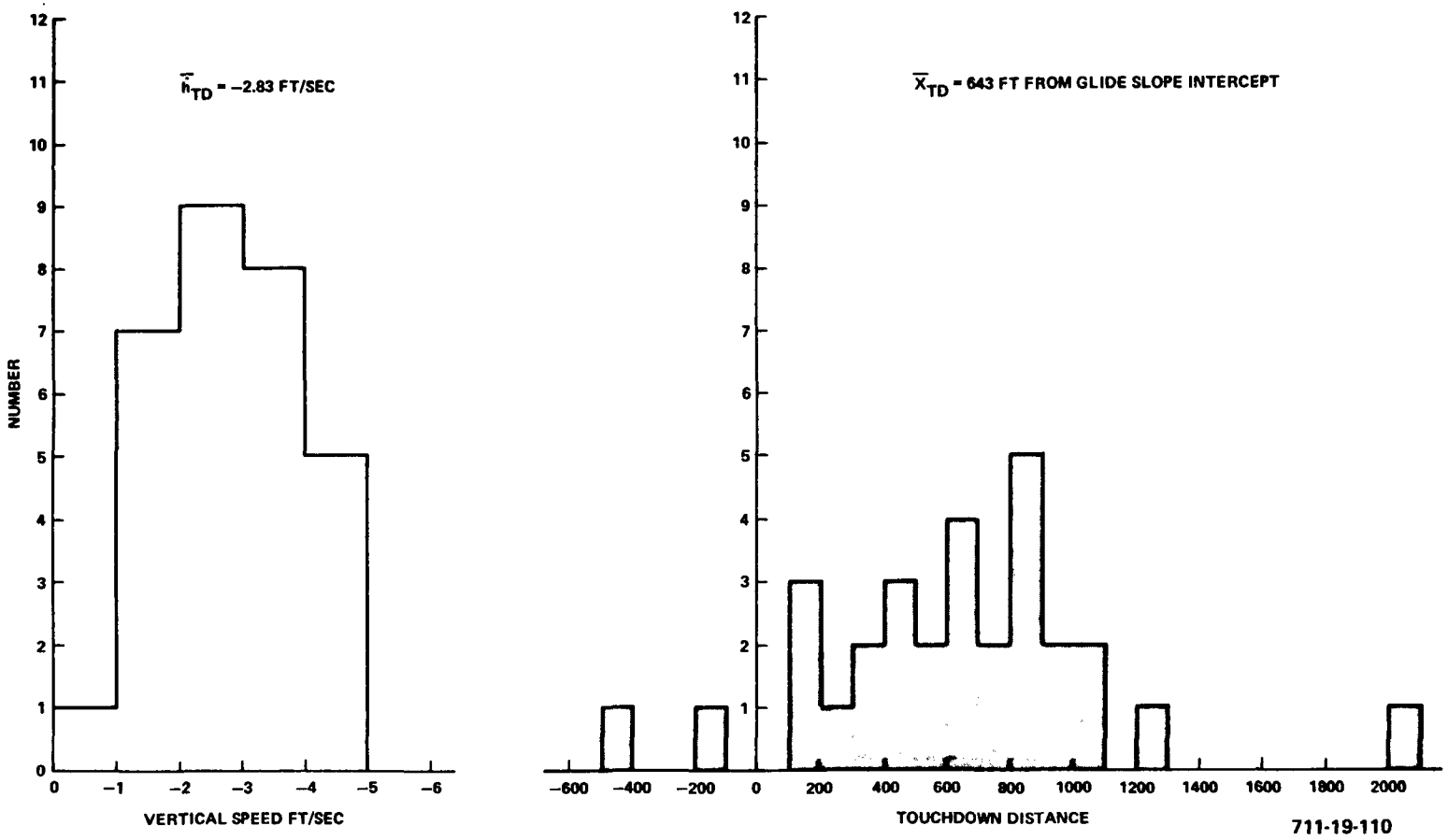

Figure 2-11
Landing Histogram, 30 Landings with Wind and Turbulence

D. DECRAB GUIDANCE

The same decrab guidance laws used in previous studies were used for the MDAC vehicle.

$$\delta_{R_{COMMAND}} = \left(\psi - \psi_R\right)\left(K_D + K_R s + \frac{K_I}{s}\right) + \frac{\delta_{RP}}{\tau_2 s + 1} \tag{2-32}$$

$$-\delta_{A_{COMMAND}} = K_\phi \phi + K_p p + (\psi_R - \psi_o)\frac{K_A}{\tau_1 s + 1} \tag{2-33}$$

where

ψ_o = heading at initiation of decrab maneuver

ψ_R = runway heading

No effort was made to optimize the decrab control law gains. The same gains used for the previous studies with the NAR vehicle were also used for the MDAC vehicle. Runs with crosswinds were not taken, but crab angles resulting from turbulence were present. Typical lateral dispersions were a few feet, but no y and $\dot{y}$ data at touchdown were recorded to determine lateral dispersion statistics. The gains used were:

$K_A = 1.73$	$K_p = 2.5$	$\delta_{RP} = 0$
$\tau_1 = 1.0$ sec	$K_R = 2.5$	τ_2 (not used)
$K_\phi = 2.5$	$K_I = 0$	

E. PARAMETRIC STUDY OF L/D EFFECTS

1. Simulation of Variable L/D

Although the MDAC vehicle was used as a baseline for these studies, the intent of the studies was to determine the guidance law sensitivity to L/D and other pertinent aero characteristics, which may be encountered in the general class of delta wing configurations. The simulation model was set up to introduce any desired variations into the lift and drag. Since the simulation equations

are written in body axis coordinates, the delta lift, and drag parameters must be resolved as follows:

- Rotate the body parameters C_A and C_N into stability axes and introduce the delta C_L and C_D.
- Rotate the incremented C_L and C_D back to body axes to obtain a new set of normal and axial force coefficients (C_A' and C_N')

$$\begin{bmatrix} C_N \\ C_A \end{bmatrix} = \begin{bmatrix} \cos\alpha & \sin\alpha \\ -\sin\alpha & \cos\alpha \end{bmatrix} \begin{bmatrix} C_L \\ C_D \end{bmatrix} \tag{2-34}$$

If we increment C_L by Δ and C_D by γ, the new components C_N' and C_A' become

$$\begin{bmatrix} C_N' \\ C_A' \end{bmatrix} = \begin{bmatrix} \cos\alpha & \sin\alpha \\ -\sin\alpha & \cos\alpha \end{bmatrix} \begin{bmatrix} (1+\Delta)\ C_L \\ (1+\gamma)\ C_D \end{bmatrix} \tag{2-35}$$

Replacing C_L and C_D by the original C_N and C_A relationship, we obtain

$$\begin{bmatrix} C_N' \\ C_A' \end{bmatrix} = \begin{bmatrix} \cos\alpha & \sin\alpha \\ -\sin\alpha & \cos\alpha \end{bmatrix} \begin{bmatrix} (1+\Delta)\ (C_N \cos\alpha - C_A \sin\alpha) \\ (1+\gamma)\ (C_N \sin\alpha + C_A \cos\alpha) \end{bmatrix} \tag{2-36}$$

After performing the multiplication and collecting terms, the relationship becomes

$$C_N' = C_N\ (1 + \Delta \cos^2\alpha + \gamma \sin^2\alpha) + C_A\ (\gamma - \Delta)\ \cos\alpha \sin\alpha \tag{2-37}$$

$$C_A' = C_A\ (1 + \Delta \sin^2\alpha + \gamma \cos^2\alpha) + C_N\ (\gamma - \Delta)\ \cos\alpha \sin\alpha \tag{2-38}$$

which was incorporated into the simulation.

2. Parametric Studies of Landing Performance

a. Introduction

The objectives of the simulator studies, in which L/D is varied, are twofold. First, we wish to determine the sensitivity of the guidance design to uncertainties in vehicle L/D characteristics. Second, we would like to establish a methodology for selecting the flight path geometry on the basis of vehicle L/D. In the first category, the simulation results to be described subsequently, provide a very complete documentation of the guidance system performance in the presence of headwinds and tailwinds with variations in L/D (about the MDAC nominal). In the second category, the establishment of a methodology for selecting glide path geometry, there were no definitive conclusions because of uncertainties in operational criteria. These uncertainties are primarily related to the tradeoff of higher approach speeds and higher approach angles versus shorter durations on the shallow glide path.

The effect of L/D variation on guidance system performance can be deduced from its effect on the equilibrium glide versus airspeed characteristics. This is illustrated qualitatively in Figure 2-12. Shown on this figure are a typical nominal flight path angle versus airspeed curve and two curves representing the effect of reducing L/D. In one case, L/D is reduced by increasing C_D. In the other case, L/D is reduced an identical amount by decreasing C_L. These curves show that drag increase has a more significant effect on the speed and glide angle relationships than lift decrease for an equivalent change in L/D. Consider a -12-degree glide angle on Figure 2-12. In the nominal case (A) the equilibrium speed is about 270 knots. If L/D is reduced by decreasing C_L (B) the -12 degree glide angle results in an equilibrium speed of about 260 knots. However, if L/D is reduced the same amount but by increasing C_D (C) then the equilibrium speed is reduced to 237 knots.

In the simulations performed to study these effects, the L/D of the MDAC vehicle was varied ±30 percent by changing both C_L and C_D. Landings on the nominal flight paths were run with the following touchdown parameters observed as the essential measurements of performance:

- Vertical Speed ($\dot{h}$)
- Touchdown Distance from Glide Path Intercept and from End of Runway

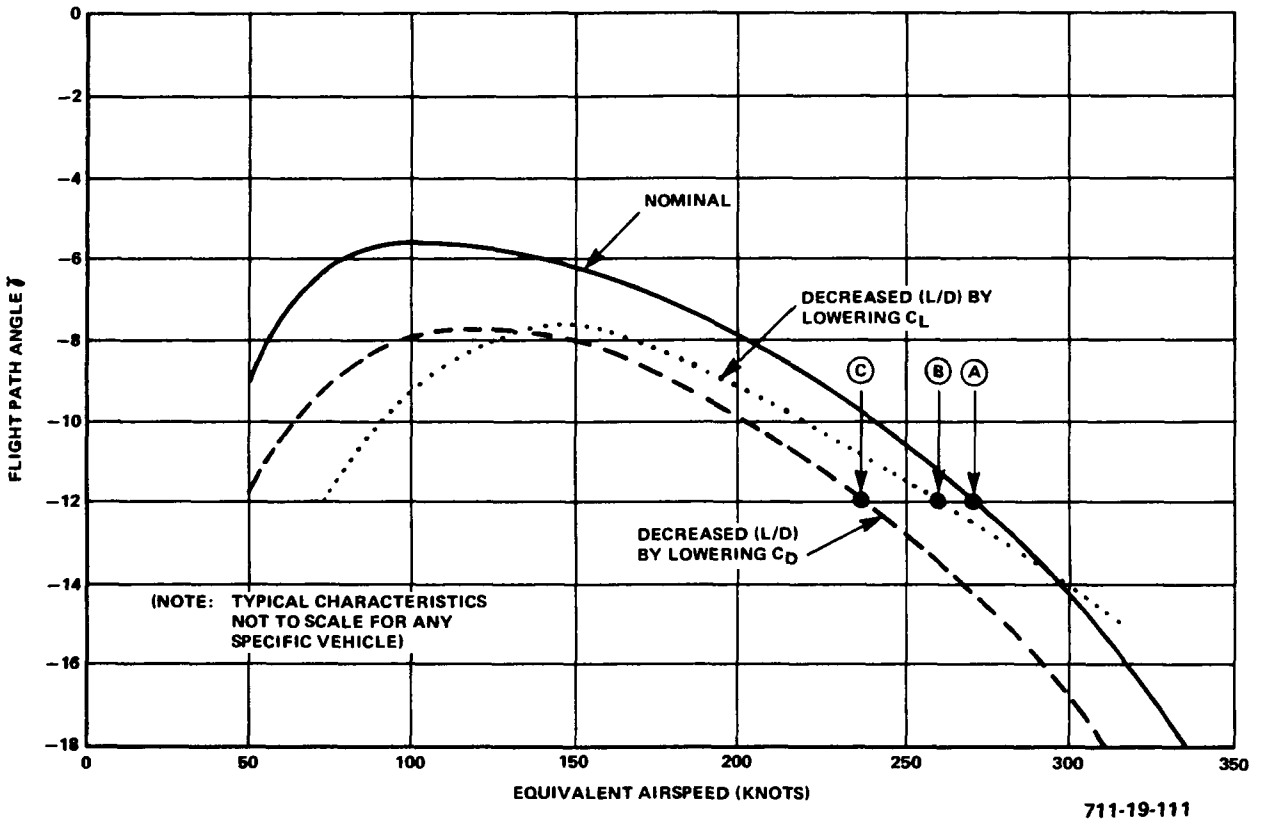

Figure 2-12
Effect of L/D Change on Equilibrium Glide versus Speed Characteristics
(Hypothetical Vehicle)

- Angle of Attack
- Ground Speed

Flights were made with winds varying between 40-knot tailwind and 40-knot headwind in 10-knot intervals.

b. Simulation Results

The simulator results are documented in Figures 2-13 through 2-20. Table 2-3 summarizes the information contained in these figures.

TABLE 2-3

SIMULATOR RESULTS FOR PARAMETRIC VARIATION OF (L/D)

Figure	Observed Parameter	Type of L/D Variation	Comments
2-13	X-Dispersion versus Winds	+30%, -20% (C_D)	Decreased (L/D) with headwinds are critical
2-14	X-Dispersion versus Winds	+30%, -20% (C_L)	Same as above, but not as critical for -L/D more critical for +(L/D)
2-15	α versus Winds	+30%, -20% (C_D)	Decreased (L/D) above 10% with headwinds are unacceptable
2-16	α versus Winds	+30%, -20% (C_L)	Same as above, but not as critical
2-17	$\dot{h}$ versus Winds	+30%, -20% (C_D)	Insensitive to increased (L/D), cannot cope with (L/D) decrease above 10%
2-18	$\dot{h}$ versus Winds	+30%, -20% (C_L)	Same as above, but not as critical
2-19	V (ground speed) versus Winds	+30%, -20% (C_D)	Excessive speed reduction for headwinds and L/D reductions greater than 10%
2-20	V (ground speed) versus Winds	+30%, -20% (C_L)	Same as above, but not as critical

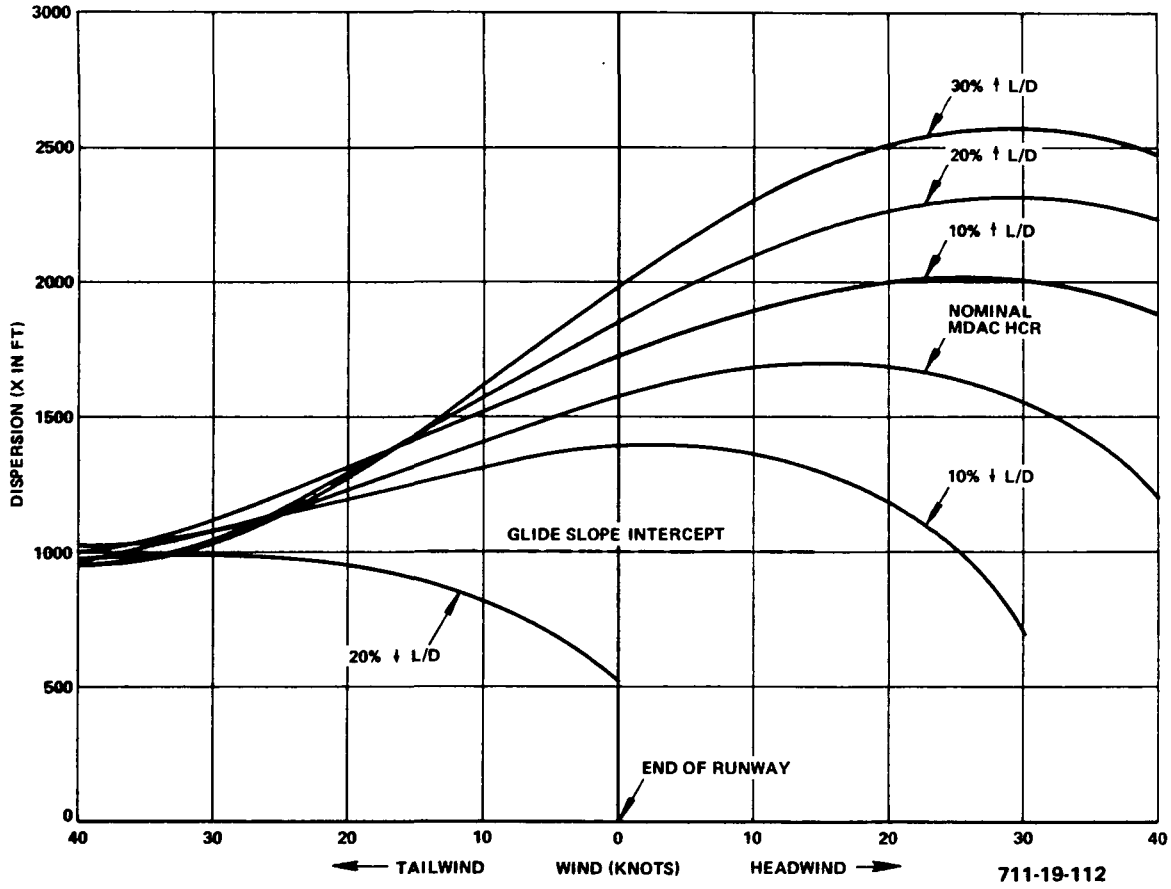

Figure 2-13
Touchdown Dispersion Down Runway versus Wind for Variations in L/D on MDAC HCR Vehicle (L/D Varied by Changes in C_D)

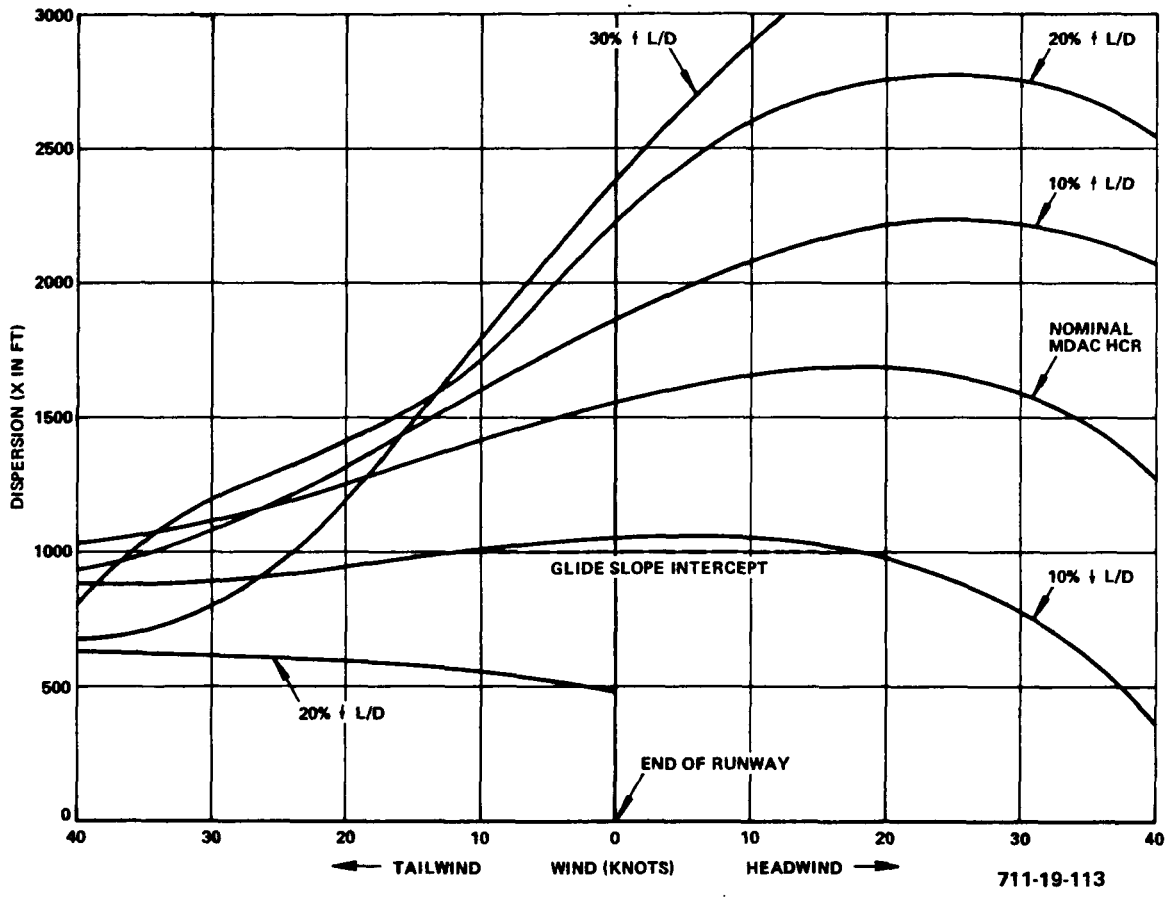

Figure 2-14
Touchdown Dispersion Down Runway versus Wind for Variations in L/D on MDAC HCR Vehicle (L/D Varied by Changes in C_L)

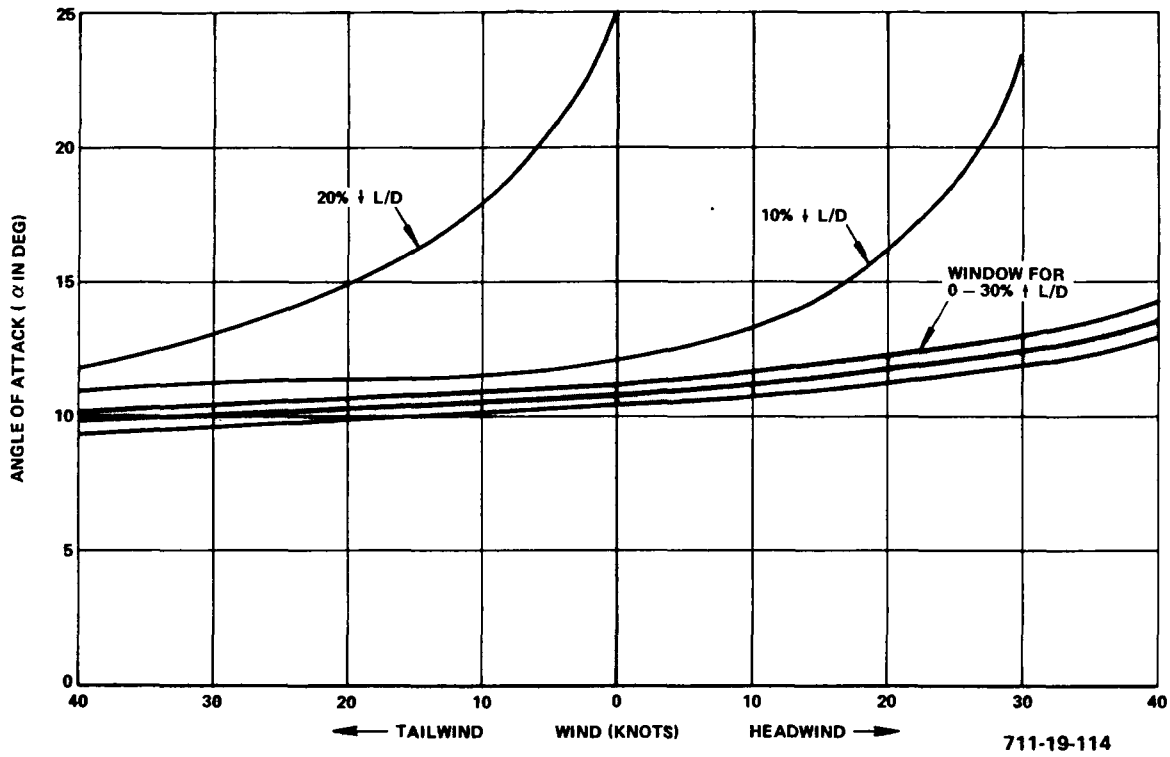

Figure 2-15
Angle of Attack at Touchdown versus Wind for Variations in L/D on MDAC HCR Vehicle (L/D Varied by Changing C_D)

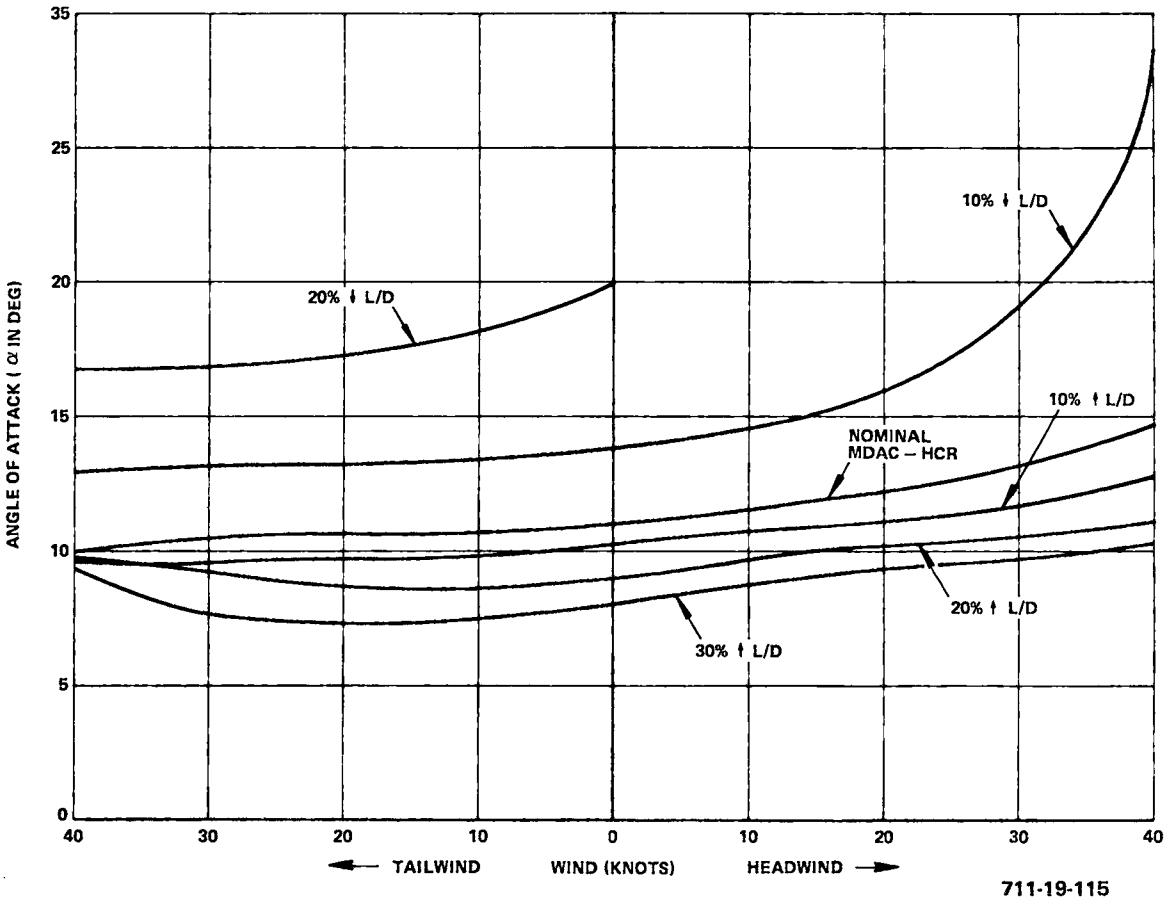

Figure 2-16
Angle of Attack at Touchdown versus Wind for Variations in L/D on MDAC HCR Vehicle (L/D Varied by Changing C_L)

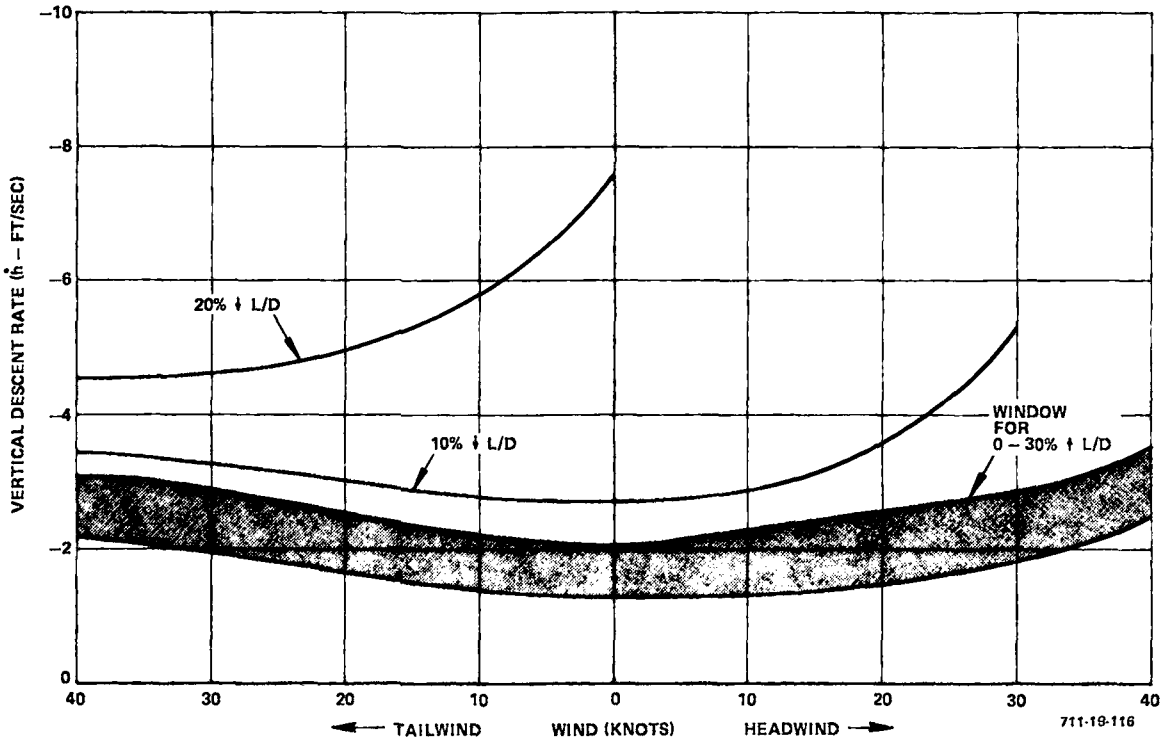

Figure 2-17
Vertical Descent Rate at Touchdown versus Wind for Variations in L/D on MDAC HCR Vehicle (L/D Varied by Changing C_D)

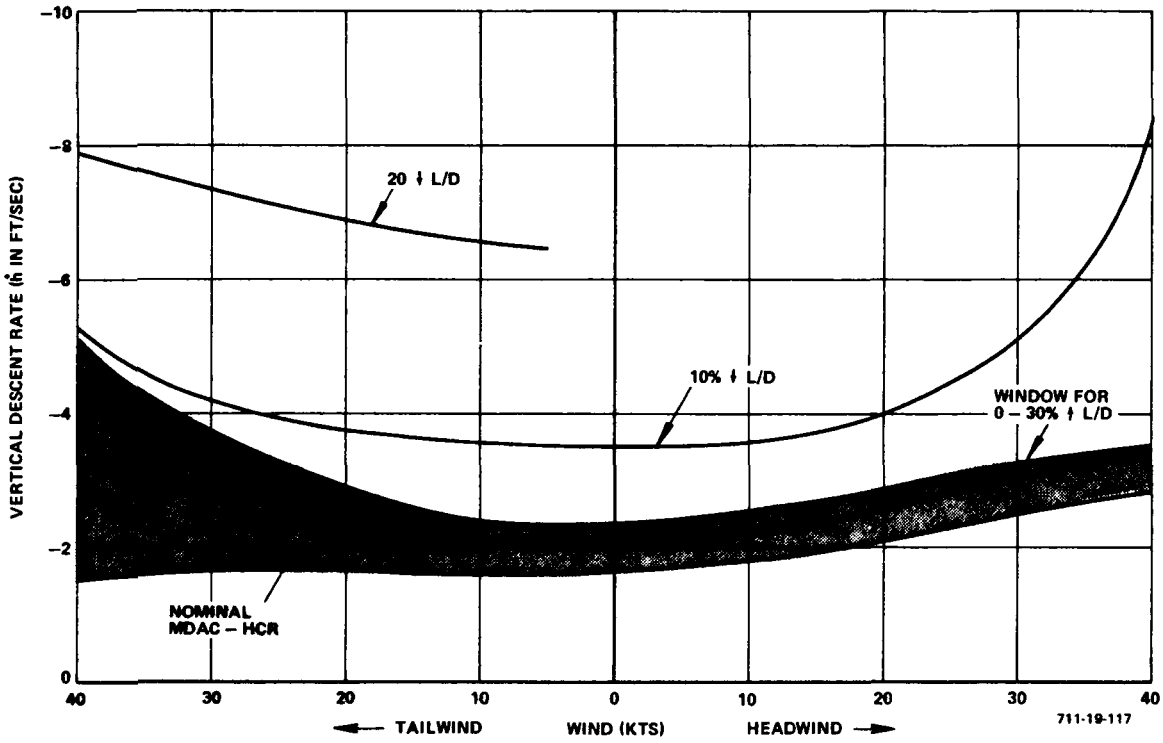

Figure 2-18
Vertical Descent Rate at Touchdown versus Wind for Variations in L/D on MDAC HCR Vehicle (L/D Varied by Changing C_L)

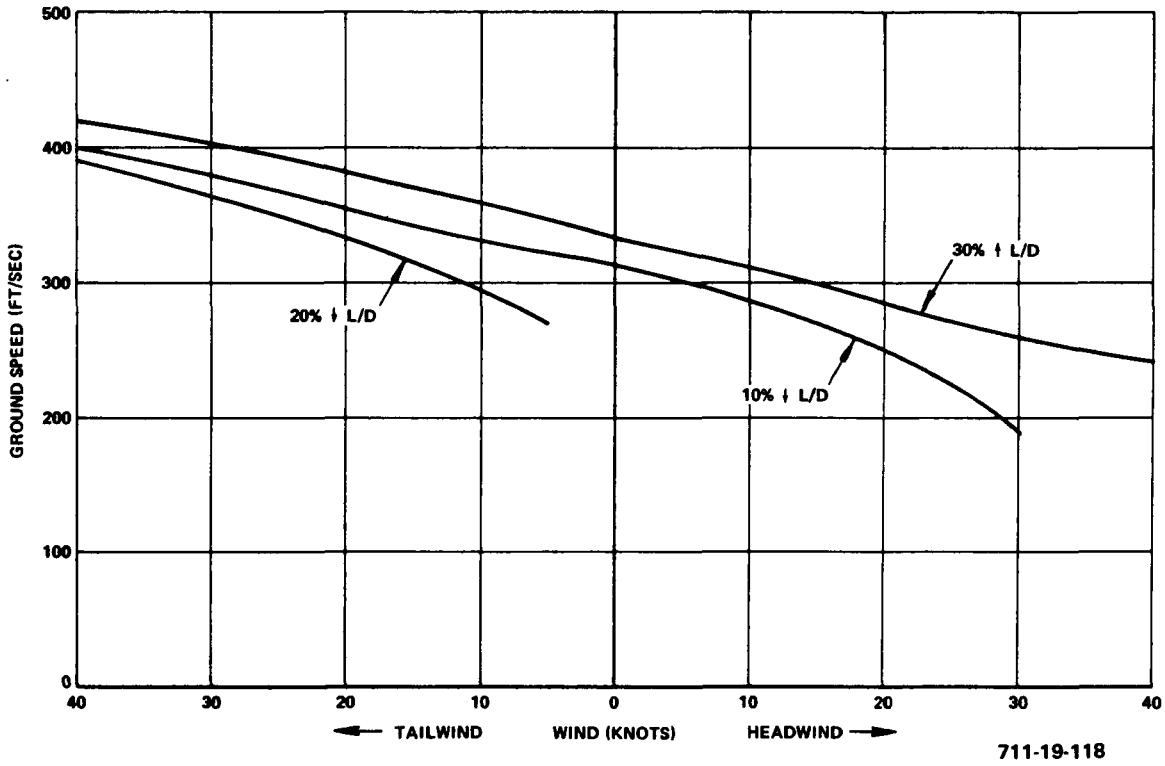

Figure 2-19
Ground Speed at Touchdown versus Wind for Variations in L/D on MDAC HCR (L/D Varied by Changing C_D)

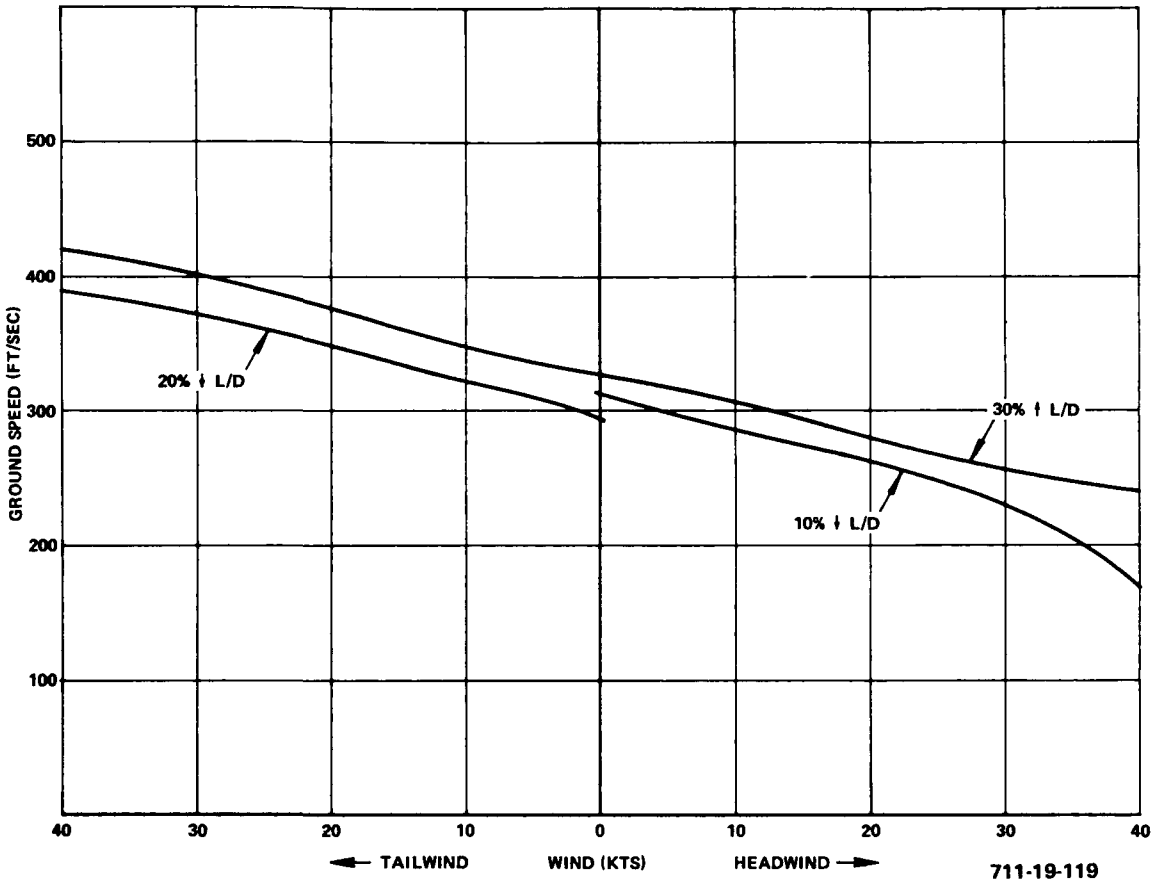

Figure 2-20
Ground Speed at Touchdown versus Wind for Variations in L/D on MDAC HCR (L/D Varied by Changing C_L)

The significant points illustrated by Figures 2-13 through 2-20 are that the guidance laws and a fixed glide path geometry are insensitive to increases in vehicle L/D. The only parameter that is not fully satisfactory for L/D increases up to 30 percent is the touchdown distance (x) in headwinds. However, the system does not cope well with decreased (L/D)'s in the presence of headwinds. This is to be expected since the headwind case is normally a lower energy final approach, and the decreased L/D also results in a lowered equilibrium speed. The decreased ground speed associated with headwind flight results in a longer duration traverse on the shallow glide path which has the effect of increasing the deceleration time. All of these factors combine to cause the speed at final flareout to tend toward excessively low values. The only sure solution to this type of problem is to alter the glide path geometry for lower L/D vehicles.

c. Glide Path Geometry Alteration

Figure 2-21 illustrates how the glide slope geometry should be altered to cope with changes in vehicle L/D about a nominal value. Consider the case of a decrease in L/D. Two procedures are possible. The glide angle may be increased to restore the equilibrium speed (or speed at first flare) to the nominal value. If this is done, the lower L/D along the shallow glide path will still result in a greater deceleration and less maneuvering margin for the final flareout. Thus, in addition to changing the steep glide path angle, the intercept with the shallow glide path should also be moved forward (toward the touchdown point).

Another method of compensating for the change in L/D is to retain the original glide angle and move the intersection of the two glide paths forward or backward for decreased or increased L/D, respectively. This changes the time on the shallow glide path so that at final flareout, the desired speeds are still achieved (providing adequate maneuvering margin still exists with the reduced L/D case).

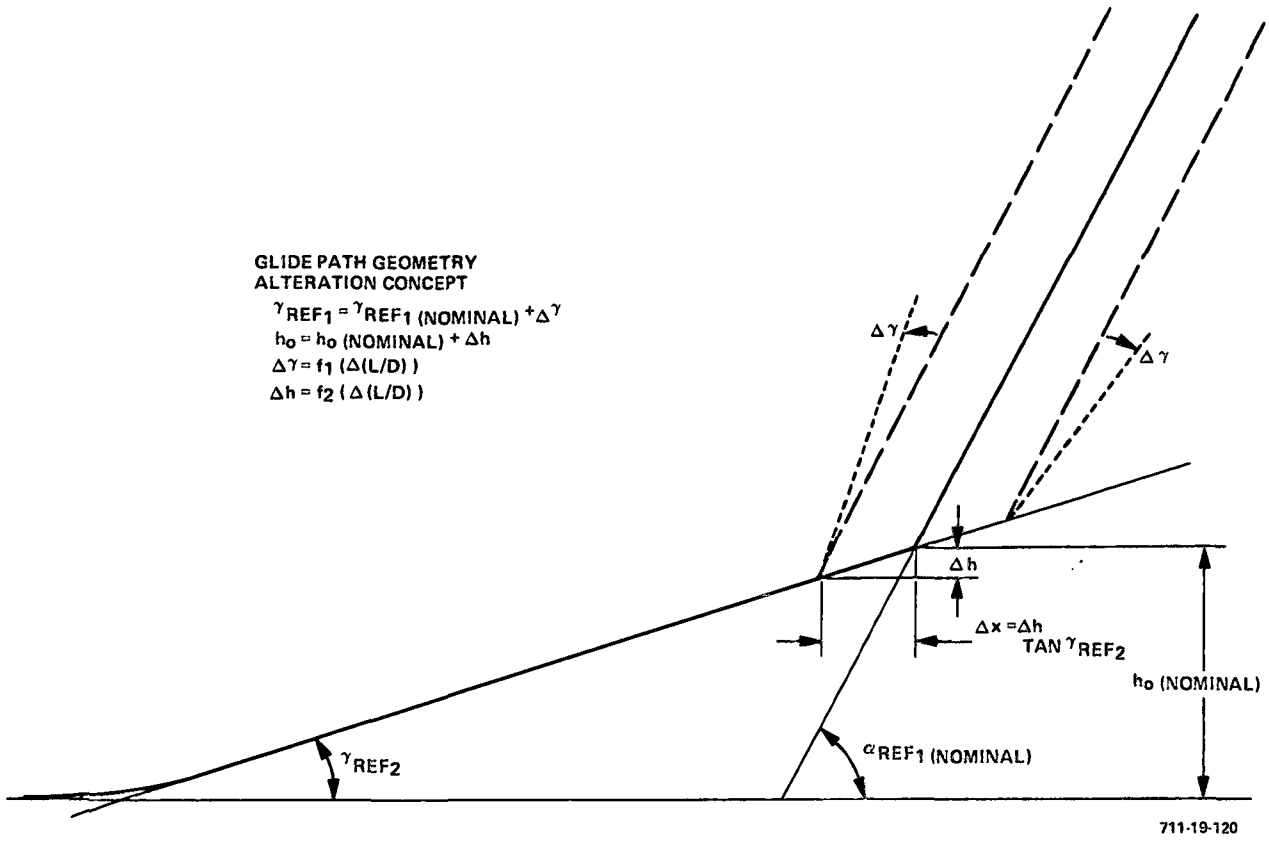

Figure 2-21
Glide Path Geometry Alteration for Vehicles with Different L/D's

Either adjusting γ_{REF_1} or adjusting the point of intersection of the two glide paths can achieve the desired compensation for a nondisturbed environment. However, a combination of the two methods might produce the best system in terms of coping with headwinds, tailwinds, wind shears, and turbulence. An investigation to determine an optimum combination of the $\Delta\gamma$ and Δh correction on Figure 2-21 was beyond the scope of this study, but it appears to be an interesting task for future work in this area. Simulator runs were taken in which Δh of Figure 2-21 was determined on the basis of reaching the final flareout altitude at the desired nominal velocity. The Δh equation determined in this manner was:

$$\Delta h = \frac{\frac{\partial h_o}{\partial (L/D)}}{L/D} \left(\frac{\Delta_{L/D}}{L/D}\right)$$

where

$$\frac{\frac{\partial h_o}{\partial (L/D)}}{L/D} = 20 \text{ ft per } 1.0\% \text{ change in } (L/D)$$

SECTION III

CONCLUSIONS

1. The guidance and control laws used in previous simulator evaluations with the NAR delta orbiter were applicable to the MDAC delta orbiter with only minor gain changes.

2. The lower subsonic L/D of the MDAC vehicle (compared to the NAR vehicle used in the previous studies) necessitated an increase in the steep glide path angle from -10 to -12 degrees. This steeper angle was needed to yield sufficient speed for tracking the shallow glide path for several hundred feet.

3. Improvements in the flareout guidance laws that adjust the predictive commands as a function if initial vertical speed and forward speed errors can reduce touchdown vertical speed dispersions in the presence of steady winds by a factor of about 2:1.

4. Speed brakes can be used to minimize dispersions resulting from headwinds and tailwinds. If the speedbrakes are deployed with a nominal deflection to cope with speed errors of both polarities, L/D is sacrificed and the use of the shallow glide path is reduced. If a traverse covering a few hundred feet of altitude on the shallow glide path is desired, then the speedbrakes should be controlled only to reduce speed increases.

5. With the statistical sample limited to 30 landings, flareout performance in the presence of winds and turbulence was:

- $\bar{\dot{h}}_{TOUCHDOWN}$ = mean touchdown $\dot{h}$ = -2.8 feet per second
- Maximum $\dot{h}_{TOUCHDOWN} < 5$ feet per second
- Nominal touchdown distance from shallow glide path intercept with the ground, x_{NOM} = 800 feet
- Estimated 2-sigma dispersion of x from x_{NOM} = 800 feet. The distribution is skewed to favor touchdowns that are short of the 800 feet nominal point.

6. The nominal guidance and control system and the selected glide path geometry for the MDAC vehicle can give acceptable landing performance if the vehicle L/D is allowed to vary +30 and -10 percent and headwinds or tailwinds are as high as 40 knots.

7. Negative L/D variations greater than -10 percent result in excessively low speeds, unacceptable angles of attack, and landings short of the runway when headwinds are present.

8. Glide path geometry can be altered to cope with different vehicle L/D's. Alteration involves changing the shallow and steep glide path intercept point and changing the angle of the steep glide path. A typical adjustment parameter is 20 feet variation in the altitude of the intersection of the two glide paths for each 1.0-percent change in vehicle L/D.

REFERENCES

1. Mueller, George E. "The New Future for Manned Spacecraft Developments", Astronautics and Aeronautics, Volume 7, No. 3, March 1969.

2. Faget, Max, "Space Shuttle: A New Configuration", Astronautics and Aeronautics, Volume 8, No. 1, January 1970.

3. Myers, Dale D. "Space Transportation System Overview and Program Plans", Space Transportation System Technology Symposium, I - Aerothermodynamics and Configurations, NASA TM X-52876, Volume I.

4. Tischler, B. O. "Space Shuttle", Astronautics and Aeronautics, Volume 9, No. 2, February 1971.

5. "Integral Launch and Reentry Vehicle Systems", NASA CR-66862, McDonnell Douglas Astronautics Corporation, November 1969.

6. "Study of Integral Launch and Reentry Vehicle System", NASA CR-102102, North American Rockwell Corporation, December 1969.

7. "Space Shuttle Final Technical Report", NASA CR-102549, General Dynamics/ Convair, October 1969.

8. "Integral Launch and Reentry Vehicle", LMSC-A959837, NASA CR 102627, Lockheed Missiles and Space Corporation, December 1969.

9. "Spacemaster - A Two Stage Fully Reusable Space Transportation System", M-69-36, Martin Marietta Corporation, December 1969.

10. "Aero Design Data Book for Delta Wing Orbiter (SSV-134C)", Pub. No. DB 2.1.5-13000 North American Rockwell (Revisions and enclosures through August 1970).

11. "Orbiter Aerodynamics Data Book, Pub. No. MDC E0407, McDonnell Douglas Astronautics Company - East, June 30, 1971.

12. "Space Shuttle Orbiter Aerodynamics Data Book", LMSC-A966076, Lockheed Missiles and Space Company, Revised 5/1/70.

13. Yoder, J. F., TRW Systems Group (Houston), "Aerodynamics Data for MSC Orbiter 245", TRW Memorandum Report 70.4353-17.

14. Behm, W. F. "Low Crossrange Orbiter Data Package", McDonnell Douglas Astronautics Company Memo No. SSPO-E241-056, August 13, 1970.

15. Dana, W. H. and Gentry, J. R. "Pilot Impressions of Lifting Body Vehicles", NASA TMX-2102, Flight Test Results Pertaining to the Space Shuttlecraft, October 1970.

16. Hoag, P. C. and Schofield, B. L. "IFR Experience with Unpowered, Low Lift-Drag Ratio Landing Approaches", NASA TMX-2102, October 1970.

17. Bray, R. S; Drinkwater III, F. J., and White, M. D. "A Flight Study of a Power-Off Landing Technique Applicable to Reentry Vehicles", NASA TN D-323, July 1960.

18. Matranga, G. J. and Armstrong, N.A. "Approach and Landing Investigation at Lift Drag Ratios of 2 to 4 Utilizing a Straight Wing Fighter Airplane", NASA TMX-31, 1959.

19. Matranga, G. J. "Analysis of X-15 Landing Approach and Flare Characteristics Determined from the First 30 Flights", NASA TN D-1057, July 1961.

20. Matranga, G. J. and Menard, J. A. "Approach and Landing Investigations at Lift-Drag Ratios of 3 to 4 Utilizing a Delta Wing Interceptor Airplane", NASA TMX-125, 1959.

21. Von Doenhoff, A. E. and Jones Jr., G. W. "An Analysis of the Power Off Landing Maneuver in Terms of the Capabilities of the Pilot and the Aerodynamic Characteristics of the Airplane", NACA TN2967, 1953.

22. Schofield, B. L. "Gliding Flight Equations", FTC-TI1M-70-1007, May 1970.

23. Osder, S. S. "Study Report, Terminal Control Energy Management and Landing of Reentry Gliders, Sperry Phoenix Company (presently Sperry Flight Systems Division) Report No. LJ-1262-0214, February 1963.

24. Schofield, B. Lyle, Richardson, D. F. and Hoag, P. C. "Terminal Area Energy Management, Approach and Landing Investigations for Maneuvering Reentry Vehicles Using F-111A and NB-52B Aircraft", Technical Document No. 70-2, USAF Flight Test Center, June 1970.

25. Kock, Berwin M. and Fulton Jr., Fitzhugh L. "Approach and Landing Studies" - Flight Test Results Pertaining to the Space Shuttlecraft, NASA TMX-2101, October 1970.

26. "Space Shuttle System Phase B Study Final Report, Part II-2A, Technical Summary - Orbiter", Report MDC E0308, McDonnell Douglas Astronautics Company, June 30, 1971.

27. Osder, S. S. "Avionics Requirements for All Weather Landing of Advanced SST's, Volume I, Analysis of System Concepts and Operational Problems and Volume II, State-of-the-Art Review of All Weather Landing System Techniques", NASA CR 73092 and CR 73093, April 1967.

28. Dendy, J. B. and Transier, K. G. "Angle of Attack Computation Study", Technical Report No. AFFDL-TR-69-93, October 1969.

29. "Simulation Handbook, Low Cross Range, Straight-Winged Orbiter (MDAC-2)", Report No. 5440-8935-S2, Sperry Flight Systems Division, September 1970.

30. "Simulation Handbook, High Cross Range Delta Wing Orbiter (North American SSV-134C)", Report No. 5440-8935-S3, Sperry Flight Systems Division, October 1970.

31. Wawrzyniak, M. E. "To What Extent Should Space Shuttle Stability and Control Be Provided Through Stability Augmentation", Space Transportation System Technology Symposium, Volume I, Aerodynamics and Configurations, NASA TMX52876, July 1970.

32. "Study Report - Equipment Mechanization and Flight Test Aircraft Selection for Space Shuttle Landing Flight Research", Report No. 70-1323-00-00, Sperry Flight Systems Division, October 1970.

APPENDIX

WIND AND TURBULENCE MODELS

1. WIND MODEL

A detailed description of the wind model used in these studies was given in Appendix B of the main report. The salient equations are repeated here. All simulations were performed using the mean wind (zero variance). The equation for the mean wind is:

$$V_{mw} = \vec{V}_o + \vec{V}_j \left[e^{-\frac{1}{2}\left(\frac{h-h_j}{D_j}\right)^2} - e^{-\frac{1}{2}\left(-\frac{h_j}{D_j}\right)^2} \right] + \vec{Sh}^2 \qquad \text{(A-1)}$$

where

$\vec{V}_o$ = low altitude wind velocity (ft/sec)

$\vec{V}_j$ = jet stream velocity (always west to east)

h_j = altitude at center of jet stream = 40,000 ft

D_j = thickness of jet stream = 13,000 ft

S = solar activity constant = 1.35×10^{-8} ft/sec/ft^2

h = altitude of vehicle (ft)

$\vec{Sh}^2$ is in the west to east direction

$$V_o = \left[\frac{(A + B \cos AMW + C \cos^2 AMW)}{D \log_{10}(10) + E} \right] V_{os} e^{-\frac{h}{H}} \left[D \log_{10}(h) + E \right] \qquad \text{(A-2)}$$

where

A = 25.317 ft/sec (15 knots)

B = 12.6585 ft/sec (7.5 knots)

C = 4.2195 ft/sec (2.5 knots)

D = 0.43

E = 0.35

H = 10,000 ft

V_{os} = Normal distribution factor that scales the level of V_o. For a mean wind $V_{os} = \frac{1}{2}$. $\left(\text{The } \sigma \text{ of the normal distribution} = \frac{1}{6}.\right)$

AMW = Angle of mean wind = 0 deg for headwind and 180 deg for tailwind.

Table A-1 summarizes the value of mean wind as derived from V_j and V_o from altitudes of 10,000 feet to about touchdown.

TABLE A-1

SUMMARY OF MEAN WIND OBTAINED FROM VECTOR SUM OF JET STREAM AND LOW ALTITUDE WINDS (Headwind Case .. AMW = 0 Degree)

h (ft)	$V_o \left(\begin{matrix}\text{AMW} = 0 \text{ deg} \\ V_{os} = 0.5\end{matrix}\right)$ (ft/sec)	V_{JET} (ft/sec)	V_{mw} (ft/sec)
10,000	20.6	13.9	34.5
7,000	27.0	7.18	34.2
5,000	31.9	4.03	35.9
4,000	34.4	2.93	37.3
2,000	42.5	1.23	43.7
1,000	40.0	0.543	40.5
500	39.0	0.255	39.3
100	32.5	0.059	32.6
10	21.1	0.0	21.1

2. TURBULENCE

Gust characteristics specified as a function of the complex variable (S) = jw are:

$$G_{u_g}(S) = \frac{\sigma_u \sqrt{\frac{2L_u}{\pi V}}}{1 + \left(\frac{L_u}{V}\right) S} \qquad \text{(A-3)}$$

$$G_{w_g}(s) = \sigma_w \sqrt{\frac{L_w}{\pi V}} \left\{ \frac{1 + \sqrt{3}\left(\frac{L_w}{V}\right) s}{\left(1 + \frac{L_w}{V} s\right)^2} \right\} \tag{A-4}$$

$$G_{v_g}(s) = \sigma_v \sqrt{\frac{L_v}{\pi V}} \left\{ \frac{1 + \sqrt{3}\left(\frac{L_v}{V}\right) s}{\left(1 + \frac{L_v}{V} s\right)^2} \right\} \tag{A-5}$$

for $h \geq 1750$ feet

$$L_u = L_v = L_w = 1750 \text{ ft} \tag{A-6}$$

for $100 \leq h < 1750$ feet

$$L_u = L_v = 145 \, (h)^{\frac{1}{3}} \tag{A-7}$$

$$L_w = h \tag{A-8}$$

for $h < 100$ feet

$$L_u = L_v = 145 \, (100)^{\frac{1}{3}} \tag{A-9}$$

$$L_w = h \tag{A-10}$$

When a value for σ_u, σ_w, and σ_v is applied to equations (A-3), (A-4) and (A-5), the turbulence simulation will provide random gusts having the desired frequency spectra and having an rms value equal to the specified σ_u, σ_w and σ_v. These sigmas are in turn specified as random variables. For example, at $h \leq 100$ feet, the 3-sigma value of σ_u is 6.8 feet per second. For the simulations performed in this study, the 2-sigma values of σ_u, σ_v and σ_w were used. Thus, below 100 feet, σ_u was (2/3) (6.8) = 4.54 feet per second. The complete specification of σ_u, σ_v and σ_w at all altitudes was:

$$0 < h \leq 100 \text{ ft}; \; \sigma_u = \left(\frac{2}{3}\right)\left(6.8\right) = 4.54 \text{ ft/sec}$$

$$100 < h \leq 60{,}000 \text{ ft}; \quad \sigma_u = \left(\frac{2}{3}\right)\left(8.24 - 0.720 \log_{10}\right)h$$

$$90{,}000 < h \leq 600{,}000 \text{ ft}; \quad \sigma_u = \left(\frac{2}{3}\right)\left(135 - 27.259 \log_{10}\right)h$$

σ_w and σ_u are defined from equations (A-6) through (A-10).